NACA

RESEARCH MEMORANDUM

EFFECT OF LONGITUDINAL WING POSITION ON THE PRESSURE CHARACTERISTICS AT TRANSONIC SPEEDS OF A 45° SWEPTBACK WING-FUSELAGE MODEL

By William Solomon and James W. Schmeer

Langley Aeronautical Laboratory
Langley Field, Va.

NATIONAL ADVISORY COMMITTEE FOR AERONAUTICS

WASHINGTON

March 4, 1953

NATIONAL ADVISORY COMMITTEE FOR AERONAUTICS

RESEARCH MEMORANDUM

EFFECT OF LONGITUDINAL WING POSITION ON THE PRESSURE CHARACTERISTICS AT TRANSONIC SPEEDS OF A 45° SWEPTBACK WING-FUSELAGE MODEL

By William Solomon and James W. Schmeer

SUMMARY

An investigation was made of the pressures at transonic speeds over a 45° sweptback wing-fuselage model. A wing of aspect ratio 4, taper ratio 0.6, having NACA 65A006 airfoil sections was tested in combination with a blunt-tail body of revolution of fineness ratio 10. The wing had two longitudinal locations: the wing-normal location, having the quarter chord of the wing mean aerodynamic chord at the 60-percent fuselage station, and wing-aft location, at the 82-percent station. Tests were made at angles of attack from -2° to 26° within a Mach number range of 0.60 to 1.03.

Analysis of the test results indicated that differences in the strength and location of the downstream shocks, resulting from wing-position change, produced changes in spanwise distribution of forces, moments, and loading upon the wing. The wing-aft configuration had the lower section normal force and wing loading and the more positive section pitching moment, especially near the wing tip. These differences increased with speed to a maximum at a Mach number of 0.98 and then decreased as stream velocities became supersonic.

Below a Mach number of 0.98, wing pressure drag at zero lift was the lesser and fuselage pressure drag the greater for the wing-aft configuration so that nearly equal pressure drag resulted for the two configurations. When the difference in wing pressure drag decreased at supersonic speeds, the wing-aft model developed somewhat greater pressure drag.

INTRODUCTION

Sweepback of wings was introduced to help alleviate the airfoil drag problem produced by the approach of flight speeds to sonic velocity.

Wing sweepback, however, introduced drag, stability, and loading problems peculiar to the swept-wing configuration. It had been found in early investigations in the transonic speed range (refs. 1 and 2) that rearward location of the swept wing on a fuselage apparently held promise for the reduction of drag of a wing-fuselage combination. Since only the effect upon zero lift drag was investigated in these preliminary tests, it was decided to investigate further the effect of wing position in the Langley 16-foot transonic tunnel over a range of lift coefficient using both force and pressure measurements.

The force measurements in the slotted-throat 16-foot transonic tunnel on a 45° sweptback wing and fuselage combination in the transonic-flow regime were reported in reference 3. These results indicated adverse changes in the drag and in the lift characteristics with rearward location of the wings.

It is the purpose of this report to present an analysis of the pressure measurements and to present a study of the flow differences over the same two model configurations reported in reference 3. The effect on wing loading of wing position is discussed and an explanation of the causes of the force variations reported in reference 3 is presented.

SYMBOLS

b	wing span
c	wing-section chord, parallel to plane of symmetry
c_{av}	average wing chord, S/b
$\bar{c}$	mean aerodynamic chord, $\frac{2}{S}\int_0^{b/2} c^2 dy$
c_m	wing-section pitching-moment coefficient
c_n	wing-section normal-force coefficient
C_D	pressure drag coefficient
ΔC_D	incremental pressure drag coefficient, wing aft minus wing normal
C_m	pitching-moment coefficient

[redacted]

C_N	normal-force coefficient
LER	leading-edge radius
M	Mach number
p	free-stream static pressure
p_l	local static pressure
P	pressure coefficient, $\frac{p_l - p}{q}$
P_{cr}	critical pressure coefficient
q	free-stream dynamic pressure, $\frac{\rho V^2}{2}$
R	Reynolds number, $\rho V\bar{c}/\mu$
S	total wing area
V	free-stream velocity
r	fuselage radial dimension
x	longitudinal distance, positive rearward
y	lateral distance, positive to right
α	model angle of attack
μ	viscosity coefficient of air in free stream
ρ	density of air in free stream

APPARATUS AND TESTS

Apparatus

The investigation reported herein was conducted in the Langley 16-foot transonic tunnel which permitted testing from a Mach number of 0.60 continuously through the speed range to a Mach number of 1.03. For details of the test section configuration and of the calibration, including longitudinal Mach number uniformity, see reference 4.

[redacted]

As reported in reference 3, the basic model for this investigation has a 45° sweptback steel wing of 0.6 taper ratio and aspect ratio 4 in combination with a blunt-tail body of revolution of fineness-ratio 10 (fig. 1). The investigation of forces (ref. 3) and of pressure characteristics reported herein were conducted simultaneously. The airfoil sections used in the wing are NACA 65A006 in a direction parallel to the plane of symmetry. For the basic model configuration, referred to as wing-normal configuration, the quarter-chord point of the wing mean aerodynamic chord is located at the longitudinal position of the fuselage maximum diameter, the 60-percent fuselage station. For the modified configuration, referred to as wing-aft configuration, the quarter-chord point is located at the 82-percent fuselage station. The change to the wing-aft configuration was accomplished by moving the body forward on the sting, the wing remaining stationary. In an attempt to have duplicate physical conditions at the base for the two configurations, a conical sleeve was attached to the sting for the wing-aft configuration.

Pressures were measured at seven spanwise stations on the wing, each having 45 orifices, and at four stations on the fuselage, each having 25 orifices. Details of the orifice locations are shown to the right of figure 1. All orifice pressures were measured by mercury manometers; the wing orifice pressures were applied also to two groups of electronic integrators, one providing section normal force and one providing section pitching moment at each station. Photographs of the manometers and printed records of the integrated values were obtained simultaneously.

Test Procedure

The range of angle of attack tested was -2° to 26° within the test program Mach number range of 0.60 to 1.03. Load limits of the sting apparatus prevented testing over the entire angle-of-attack range at all test Mach numbers. A 10° coupling, as shown in figure 2, was used at the higher angles of attack tested.

In order to minimize the movement of the model from stream center with angle-of-attack change, the axis of rotation of the model was located at the longitudinal station corresponding to the quarter-chord point of the mean aerodynamic chord. Figure 2 illustrates the model mounting in the 16-foot slotted-throat tunnel showing the angle-of-attack mechanism, the model position for straight and 10° coupling, and the relative position of the axis of rotation. The model angle of attack was set during the tests to allow for the deflection of the sting under load. For details of this procedure, see reference 3.

The Reynolds number obtained over the Mach number range tested is shown in figure 3.

[redacted]

Corrections

The slotted-wall test section tends to nullify the interference effects upon which are based the usual wind-tunnel wall corrections for subsonic compressible flow (ref. 5). It also alleviates the tunnel-wall blockage interference and choking effects and permits testing at transonic Mach numbers. Below a Mach number of 1.02 (the present test maximum is 1.03) jet-boundary-reflected compression waves have no significant interference effects on the surface pressures of nonlifting models (ref. 6). For lifting models, the interference effects have not yet been experimentally evaluated but preliminary analytical studies have indicated little effect. Therefore, no jet-boundary corrections have been applied to the data presented herein.

Because of the change in longitudinal position of the wing in this investigation, a difference exists in the proximity of the wing to the sting for the two configurations. A possibility therefore exists for a difference in sting interference. This difference was not evaluated but is believed to have small effect.

RESULTS

The normal-force and pitching-moment characteristics of the wing in the presence of the fuselage, obtained by spanwise integration of section data given by the electronic-pressure integrators, are shown in figures 4 and 5. The variation with Mach number of the longitudinal center of pressure and of the lateral center of pressure for the wing panels is shown in figure 6.

In order to assist in understanding the flow phenomena, a sketch is presented (fig. 7) showing the principal disturbances affecting the flow as represented by chordwise pressure contours in isometric view. Presented in figures 8 and 9 are the chordwise distributions of the pressure coefficients measured at the fuselage vertical plane of symmetry and at the seven wing stations. Since the principal changes apparent in the pressures over the two configurations occurred on the upper surface, some of the lower-surface wing pressures have been omitted from the isometric views in the interest of clarity. It should be noted that the same identifying lines are used for both the upper and lower surfaces of the model; the solid lines represent data obtained for the wing-normal configuration and the broken lines for the wing-aft configuration. Only those fuselage pressures at the plane of symmetry which are in the region of influence of the wing are shown, and the fuselage base position is noted to orient the wing with respect to the fuselage for the two configurations. In order to simplify the discussion, the figures giving

chordwise pressure distribution are limited to angles of attack of 0°, 4°, 8°, and 12° at Mach numbers of 0.60, 0.90, 0.94, 0.98, 1.00, and 1.02, and to 16°, 20°, and 24° at 0.60 Mach number.

These chordwise-pressure distributions provide the basis for an analysis of the difference in forces and moments experienced by each of the two configurations. The location and extent of these differences are shown in the spanwise distributions of the section normal-force and the section pitching-moment coefficients (figs. 10 and 11). The presentation of section characteristics is limited to a representative group measured at the same Mach numbers as presented for the chordwise pressure coefficients. Figure 12 presents an analysis of the difference in the pressure drag of the two configurations.

DISCUSSION

Integrated Pressure Characteristics

Differences in the integrated pressure characteristics between the wing-normal and wing-aft configurations (figs. 4 and 5) are similar to the differences in the force characteristics of the two complete model configurations reported in reference 3. At low angles of attack, the slopes of the normal-force curves (fig. 4) are somewhat less for the wing-aft configurations at all Mach numbers tested. Also, in the high-lift range and above a Mach number of 0.70, there is a loss in normal-force coefficient for the wing-aft position, this loss increasing with Mach number up to 0.98. Above a Mach number of 0.60, the wing-aft pitching-moment curves (fig. 5) have slightly more positive slope in the low-lift range. Also the wing pitch-up characteristics at normal-force coefficients of 0.55 to 0.60 tend to be more severe for the wing-aft position.

At low lift, there is a trend for the longitudinal center of pressure on the wing panel (fig. 6(a)) to be more forward for the wing-aft configuration. For the higher Mach numbers tested, a trend toward inboard movement also is noted, as seen from the curves of lateral center of pressure (fig. 6(b)). At near sonic speeds, the center of pressure for wing-aft configuration tends to be inboard and forward of the center of pressure for the wing-normal configuration. This small inboard center-of-pressure movement and the lower normal-force-curve slope for the wing-aft configuration indicates a small reduction in the wing bending moment with rearward positioning of the wing.

Chordwise Pressure Distribution

Although the changes in the over-all characteristics of the wing effected by change in wing position are small, there are distinct changes in the flow and in the spanwise and chordwise distribution of forces which are revealed by the chordwise-pressure distributions (figs. 8 and 9). Some of the more prominent flow changes are discussed in the following paragraphs, and the effect of these changes upon the spanwise distribution of normal force and pitching moment are described afterwards. The explanation of these flow changes requires an understanding of several of the disturbances which affect the flow over the wing. One disturbance, which appears first at the juncture of the fuselage and the wing trailing edge and which extends outboard with increase in airspeed, is a result of the flow deceleration at the rear of the wing at supercritical speeds. This disturbance is herein referred to as the trailing-edge shock. (See fig. 7.) A second disturbance is the shock associated with the deceleration of the supersonic flow field over the complete model; this shock is termed the decelerating-flow shock. Also indicated in figure 7 is a third disturbance, termed the leading-edge shock, which is associated with the deceleration of the supersonic expansion field (low-pressure peak region) at the leading edge. Another disturbance apparent in the chordwise pressure distributions is the shock caused by the flow discontinuity at the wing-tip leading edge, noted herein as the tip shock. For schlieren and tuft photographs as well as a discussion of the flow over a model geometrically similar to the wing-normal configuration, see reference 7.

0° angle of attack.- The wing, when in the rearward position, is seen to be located nearer a more positive pressure field of subsonic flow deceleration at the rear of the fuselage than when in the normal position (fig. 8(a)). When the flow over the entire model is subcritical, as at a Mach number of 0.60, the effect on the wing pressure distribution is negligible. At a Mach number of 0.90, small influence of the positive pressure field on the wing pressures is noted. At a Mach number of 0.94, however, the pressure contours indicate that the more positive pressure field causes the trailing-edge shock, which has developed (supercritical flow extending over most of the wing), to occur farther forward for the wing-aft configuration. This location of the trailing-edge shock results in more positive pressures over the rear of the inboard wing stations and over the entire chord from 70-percent semispan outboard for the wing-aft configuration. The positive pressure field also causes a more forward location of the tip shock (which is noted at a Mach number of 0.94) on the wing of the wing-aft configuration.

At 0.98 Mach number, the decelerating-flow shock has developed downstream of the trailing-edge shock as indicated by the fuselage pressures in figure 8(a). Moreover, the pressures indicate that this

decelerating-flow shock has developed farther forward, relative to the wing, for the wing-aft configuration. Because of the more forward location, the decelerating-flow shock combines with the trailing-edge shock at 40-percent semispan for the wing-aft configuration as compared to 95 percent for wing-normal configuration. It should be noted also that the combined shock of the wing-aft configuration is the stronger shock as evidenced by the greater pressure rise (fig. 8(a)). This condition results in more positive pressures being produced over the rear of all outboard wing stations of the wing-aft configuration. At this speed, Mach number of 0.98, the tip shock merges with the main disturbance which sweeps out to the wing tip, and any effect of wing position upon the tip shock is masked.

With further increases in Mach number, the decelerating-flow shock moves rearward and the trailing-edge shock becomes more inclined to the stream. As seen in figure 8(a), this causes the point of intersection of the two shocks to move off the wing for the wing-normal configuration and to move farther outboard and rearward along the wing for wing-aft configuration. Thus, as the wing area affected by the merger of the decelerating-flow shock with the trailing-edge shock becomes smaller for the wing-aft configuration with increase in Mach number, the differences between the pressure distributions for the two wing configurations decrease.

Also noted from figure 8(a) whenever supercritical flow exists, the trend is toward slightly lower pressures over the inboard wing sections for the wing-aft configuration. These lower pressures are induced by the accelerating supersonic flow over the contracting section of the fuselage afterbody.

4° angle of attack.- The pressure distributions for 4° angle of attack, presented in figure 8(b), show flow disturbance effects similar to those described at 0°. Again the amount of wing area affected by the decelerating-flow shock in combination with the trailing-edge shock is responsible for the principal differences in wing pressures of the two configurations. Although a leading-edge shock develops, this disturbance is not affected by wing position but appears to be mainly a function of angle of attack. The greatest effect of wing position is again observed at a Mach number of 0.98. With further increases in speed, the differences in pressures developed over the two configurations tend to diminish.

8° and 12° angles of attack.- At angles of attack of 8° and 12° (figs. 8(c) and 8(d)) thick boundary-layer and flow-separation regions develop. Nevertheless, the combination of the decelerating-flow shock with the trailing-edge shock is still responsible for the principal changes in pressures between the wing-normal configuration and the wing-aft configuration. At wing stations where separated flow exists, the

[redacted]

more positive pressures for the wing-aft configuration occur not solely at the rear of the airfoil but over the entire chord. Such a difference in pressure distribution between the two configurations results from the difference in the strength of combined shock which interacts with the thick (subsonic) boundary layer transmitting pressures upstream of the shock position. As for the lower angles of attack, the greatest pressure differences at 8° and 12° occur at a Mach number of 0.98 and tend to diminish when the speed is increased.

Higher angles of attack.- As the flow separation extends inboard with increase in angle of attack, there is only a small effect of wing position on the wing pressures at a Mach number of 0.60 as noted in figure 9. The small difference in wing pressures between the two configurations at 16°, 20°, and 24° angle of attack is the same as that observed at subcritical speeds for the lower angles of attack.

Section Normal-Force Characteristics

Although the shape of the section normal-force distribution curves (fig. 10) is similar for the two configurations at a given speed and angle of attack, there are evident changes in magnitude. Generally, the section normal-force coefficients are slightly lower for the wing-aft configuration than for the wing-normal configuration. It should be noted that the erratic behavior of the curves at 10° angle of attack is the result of intermittent separation in the flow. At supercritical speeds, Mach number of 0.94 and above, there is a marked reduction in section normal force over the outboard wing sections with rearward location of the wing. These reductions in section normal-force coefficient are the result of the more positive pressures on the upper wing surface produced by the stronger combined decelerating-flow and trailing-edge shock over the wing-aft configuration (fig. 8).

Since the wing loading of a given wing is a function of the section normal-force-coefficient distribution, the lower section normal force also indicates lower wing loading for the wing-aft configuration. In addition, the reduced loading over the outboard wing stations of the wing-aft configuration at supercritical speeds indicates a slight inboard movement of lateral center of pressure and a slight reduction in bending moment at the wing-fuselage juncture. The magnitude of the center-of-pressure movement for a few angles of attack has been shown in figure 6(b).

As seen in figure 10, the differences in section normal force (and wing loading) generally increase with angle of attack, increase with speed to a maximum at a Mach number of 0.98, and then diminish as the speeds become supersonic.

Section Pitching-Moment Characteristics

The general shape of the section pitching-moment distribution curves at a given angle of attack and Mach number is not affected by the change in wing location (fig. 11). However, a region of more positive pitching moment for the wing-aft configuration at the inboard wing stations, evident at a Mach number of 0.60, expands toward the tip with increase in Mach number to 0.98. The cause of this phenomenon is the increase with speed in the spanwise and chordwise extent and in the magnitude of the more positive pressures developed for wing-aft location, which has been observed in figure 8. For the low angles of attack, the more positive pressures over the upper surface at the rear of the wing in the rearward location produces the more positive section pitching-moment coefficients. Another result of these more positive pressures is a small forward movement of longitudinal center of pressure with rearward wing location; the magnitude of this center-of-pressure movement for several angles of attack has been shown in figure 6(a). For the wing sections with separated flow, having the more positive pressures over the entire chord, the area affected to the rear of the quarter-chord point has the greater moment so that more positive section pitching moment for the wing-aft location is produced. The difference in section pitching-moment coefficient between the two configurations decreases with increase in speed above a Mach number of 0.98 as the difference in pressure coefficient decreases (fig. 8).

Pressure Drag Coefficient

A comparison of the incremental pressure drag coefficient of the components of the two wing-fuselage configurations at 0° angle of attack is shown in figure 12. The results are obtained by subtracting the pressure drag coefficient of the wing-normal component from the pressure drag coefficient of the wing-aft component.

The lower curve of figure 12 shows that the pressure drag is less for the wing of the wing-aft configuration. This results from the forward location of the combined decelerating-flow and trailing-edge shock producing a greater area of more positive pressure at the rear of the wing for the wing-aft configuration. At a Mach number of 0.98, this pressure-drag difference approaches a maximum and then diminishes with increasing Mach number as the decelerating-flow shock moves rearward off the wing (fig. 8(a)).

The upper curve of figure 12 shows that the pressure drag is greater for the fuselage of the wing-aft configuration. This difference results from the decreased pressures over the fuselage induced by the presence of the wing at the rear of the body (fig. 8(a)) where the projected area

affected is greater for the wing-aft configuration; the wing-normal configuration has the reduced pressure region near the body maximum thickness. There is only a small variation of the fuselage incremental-pressure drag with Mach number in the transonic range tested.

The middle curve of figure 12 shows the effect of combining the wing and fuselage pressure drag results yielding substantially no difference in pressure drag between the two configurations up to a Mach number of 0.98. When the differences in wing pressure drag of the two configurations begin to diminish at near sonic speeds, the wing-aft configuration shows the higher pressure drag because of the adverse effect of the wing on the fuselage pressures.

CONCLUDING REMARKS

Analysis of the results of an investigation of the pressures at transonic speeds over a 45° sweptback wing-fuselage model, having two longitudinal locations of the wing indicates the following:

Distinct changes occur in the flow to produce changes in the spanwise distribution of forces, moments, and loading on the wing. These flow changes are apparent in the strength and in spanwise and chordwise location on the wing of the decelerating-flow shock in combination with the trailing-edge shock. For the rearward wing position (wing-aft position) compared to the normal wing position, more positive pressures are produced over the rear of the wing upper surface at low angles of attack and over the entire chord when separation occurs. This pressure difference results in lower section normal force and wing loading and in more positive section pitching moment, especially near the tip, for the wing-aft configuration. These differences increase with speed to a maximum at a Mach number of 0.98 and then decrease as stream velocities become supersonic.

At zero lift, the pressure drag of the wing is lower for the wing in the rearward position because of the more positive pressures at the rear of the wing. The difference in wing pressure drag between the two configurations approaches a maximum at a Mach number of 0.98 and then decreases as the decelerating-flow shock moves off the wing of both configurations with increase of stream velocity to supersonic. At all speeds tested, the presence of the wing produces an increased pressure drag for the fuselage of the wing-aft configuration. The difference in pressure drag for the wing is approximately of the same magnitude but of opposite sign as the difference for the fuselage (between the two configurations) below a Mach number of 0.98. Negligible pressure-drag difference between the two wing-fuselage combinations below a Mach

number of 0.98 results. At supersonic speeds, when the difference in wing pressure drag between the two configurations decreases, the wing-aft combination develops somewhat higher pressure drag.

Langley Aeronautical Laboratory,
National Advisory Committee for Aeronautics,
Langley Field, Va.

REFERENCES

1. Mathews, Charles W., and Thompson, Jim Rogers: Comparison of the Transonic Drag Characteristics of Two Wing-Body Combinations Differing Only in the Location of the 45° Sweptback Wing. NACA RM L7I01, 1947.

2. Katz, Ellis: Flight Investigation From High Subsonic to Supersonic Speeds To Determine the Zero-Lift Drag of a Transonic Research Vehicle Having Wings of 45° Sweepback, Aspect Ratio 4, Taper Ratio 0.6, and NACA 65A006 Airfoil Sections. NACA RM L9H30, 1949.

3. Hallissy, Joseph M., and Bowman, Donald R.: Transonic Characteristics of a 45° Sweptback Wing-Fuselage Combination. Effect of Longitudinal Wing Position and Division of Wing and Fuselage Forces and Moments. NACA RM L52K04, 1952.

4. Ward, Vernon G., Whitcomb, Charles F., and Pearson, Merwin D.: Air-Flow and Power Characteristics of the Langley 16-Foot Transonic Tunnel With Slotted Test Section. NACA RM L52E01, 1952.

5. Wright, Ray H., and Ward, Vernon G.: NACA Transonic Wind-Tunnel Test Sections. NACA RM L8J06, 1948.

6. Ritchie, Virgil S., and Pearson, Albin O.: Calibration of the Slotted Test Section of the Langley 8-Foot Transonic Tunnel and Preliminary Experimental Investigation of Boundary-Reflected Disturbances. NACA RM L51K14, 1952.

7. Whitcomb, Richard T., and Kelly, Thomas C.: A Study of the Flow Over a 45° Sweptback Wing-Fuselage Combination at Transonic Mach Numbers. NACA RM L52D01, 1952.

[redacted]

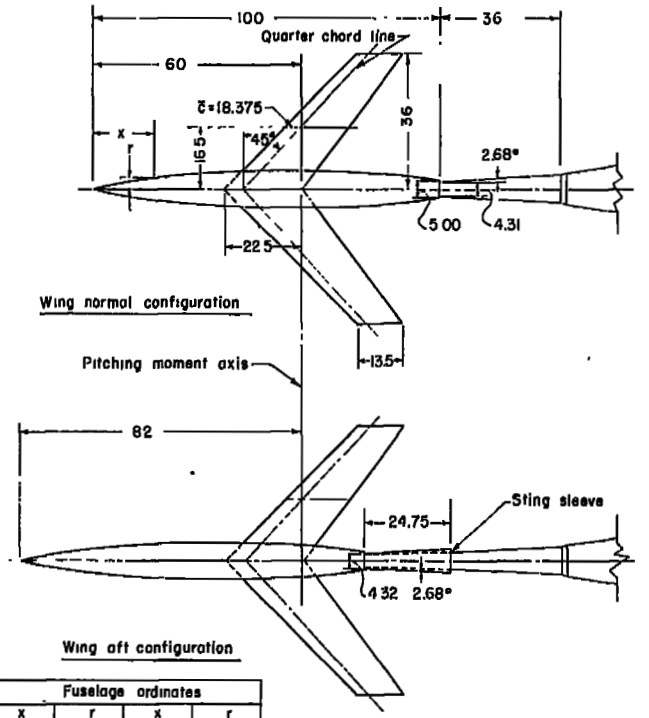

Fuselage ordinates			
x	r	x	r
0	0	42.00	4.719
0.60	0.277	48.00	4.896
0.90	.358	54.00	4.971
1.50	.514	60.00	5.000
3.00	.866	66.00	4.955
6.00	1.446	72.00	4.828
9.00	1.936	78.00	4.610
12.00	2.365	84.00	4.274
18.00	3.112	90.00	3.754
24.00	3.708	96.00	3.031
30.00	4.158	100.00	2.500
36.00	4.489	LER	0.060

Wing data	
Taper ratio	0.6
Aspect ratio	4.0
Wing area	9 sq ft
Airfoil section	NACA 65A006 parallel to plane of symmetry

Wing orifice station
Location in percent of semispan

A	13.5
B	25.0
C	40.0
D	55.0
E	70.0
F	85.0
G	95.0

Wing orifice location at each of seven stations

Percent chord	
0	45.00
1.25	50.00
2.50	55.00
5.00	60.00
7.50	65.00
10.00	70.00
15.00	75.00
20.00	80.00
25.00	85.00
30.00	90.00
35.00	95.00
40.00	

Fuselage orifice location at each of four rows

Percent length	
2.00	52.00
4.00	56.00
8.00	60.00
12.00	64.00
16.00	68.00
20.00	72.00
24.00	76.00
28.00	80.00
32.00	84.00
36.00	88.00
40.00	92.00
44.00	96.00
48.00	

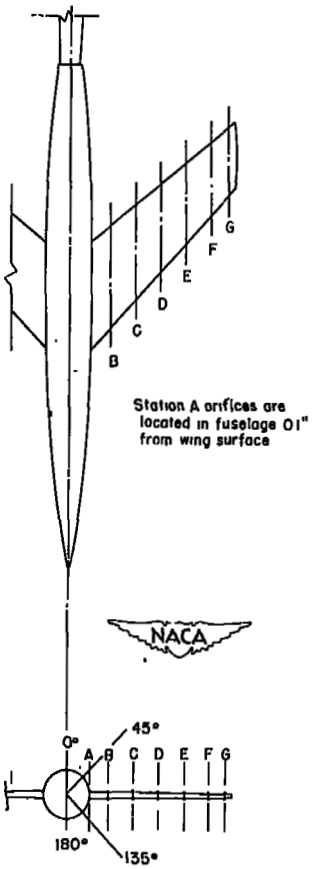

Figure 1.- Diagram of the wing-fuselage model, showing the dimensional details of the two configurations and the location of the pressure orifices. All linear dimensions are in inches.

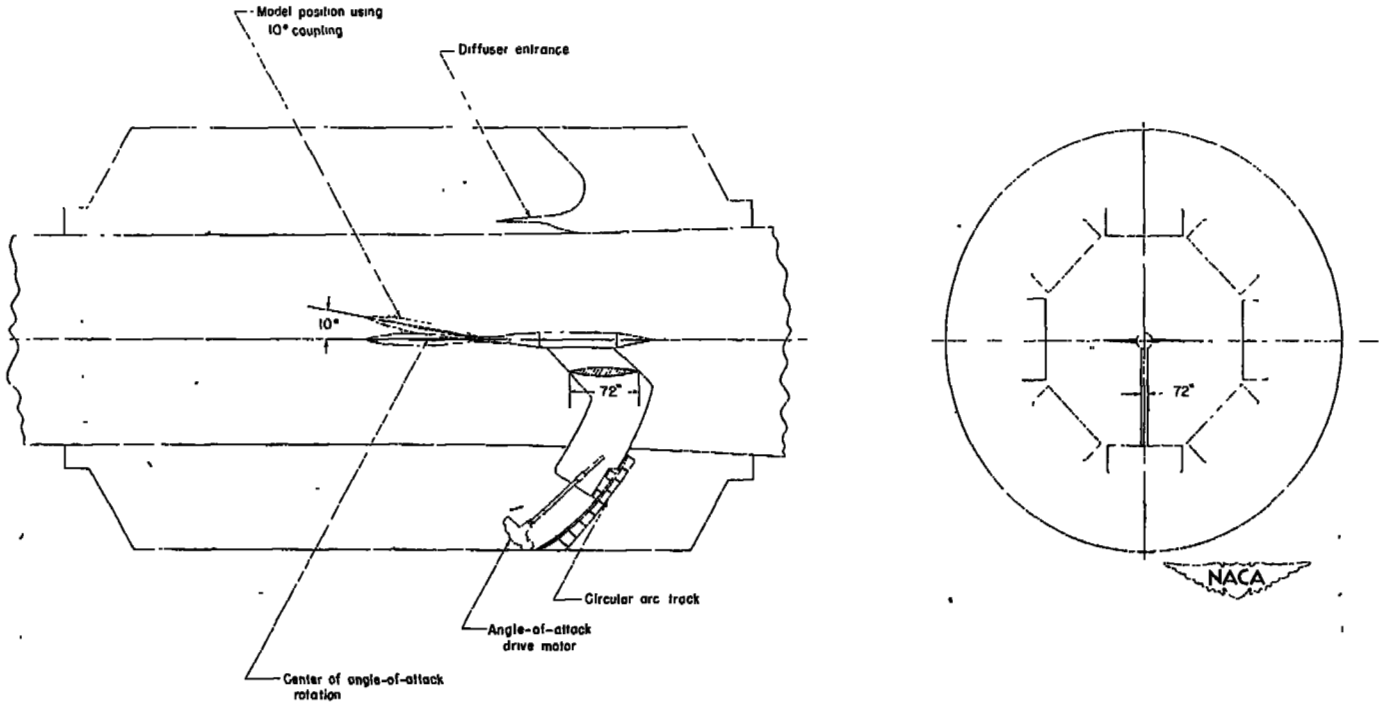

Figure 2.- Diagram of the 100-inch wing-fuselage model in the Langley 16-foot transonic tunnel showing details of the angle-of-attack mechanism.

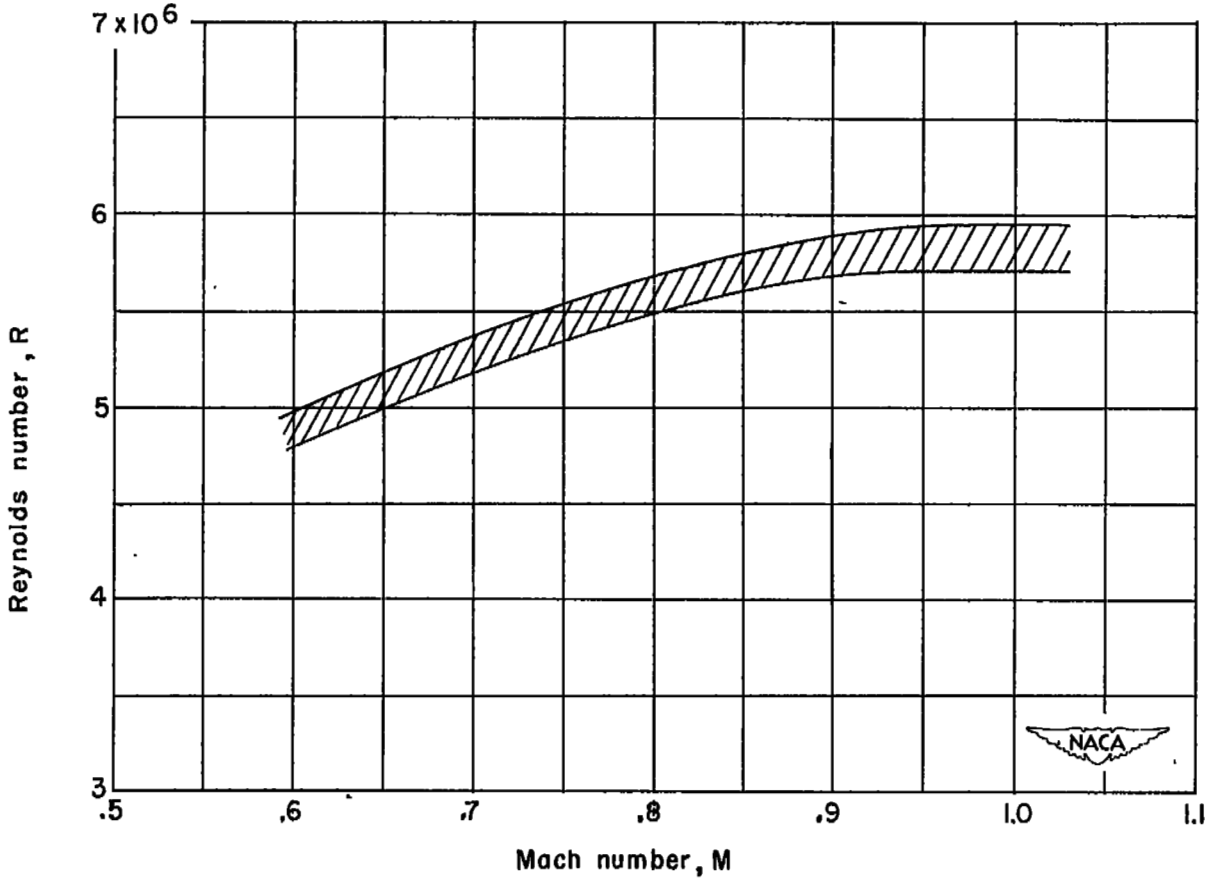

Figure 3.- Approximate Reynolds number based on mean aerodynamic chord.

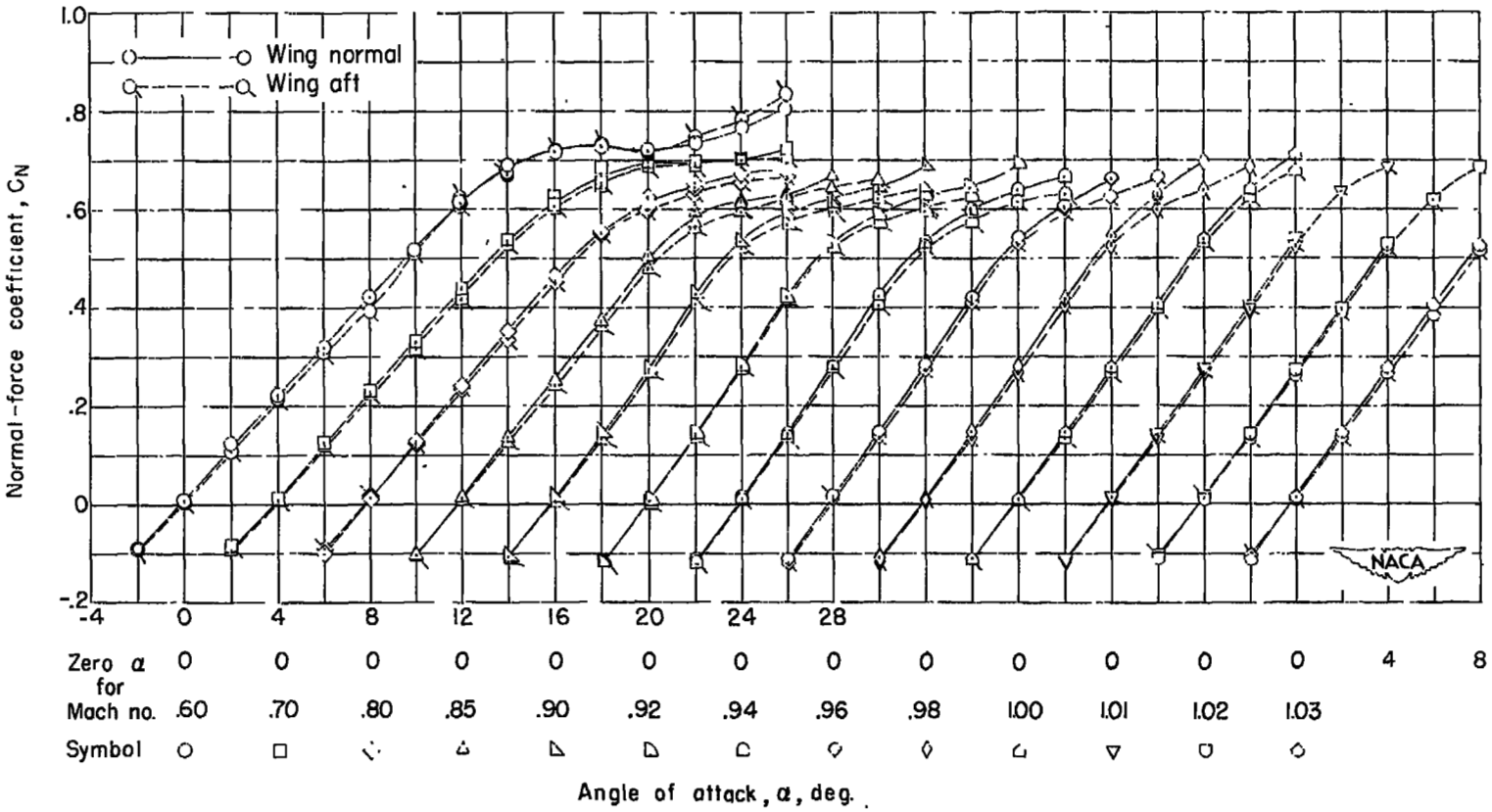

Figure 4.- The effect of wing location upon the wing normal-force coefficient.

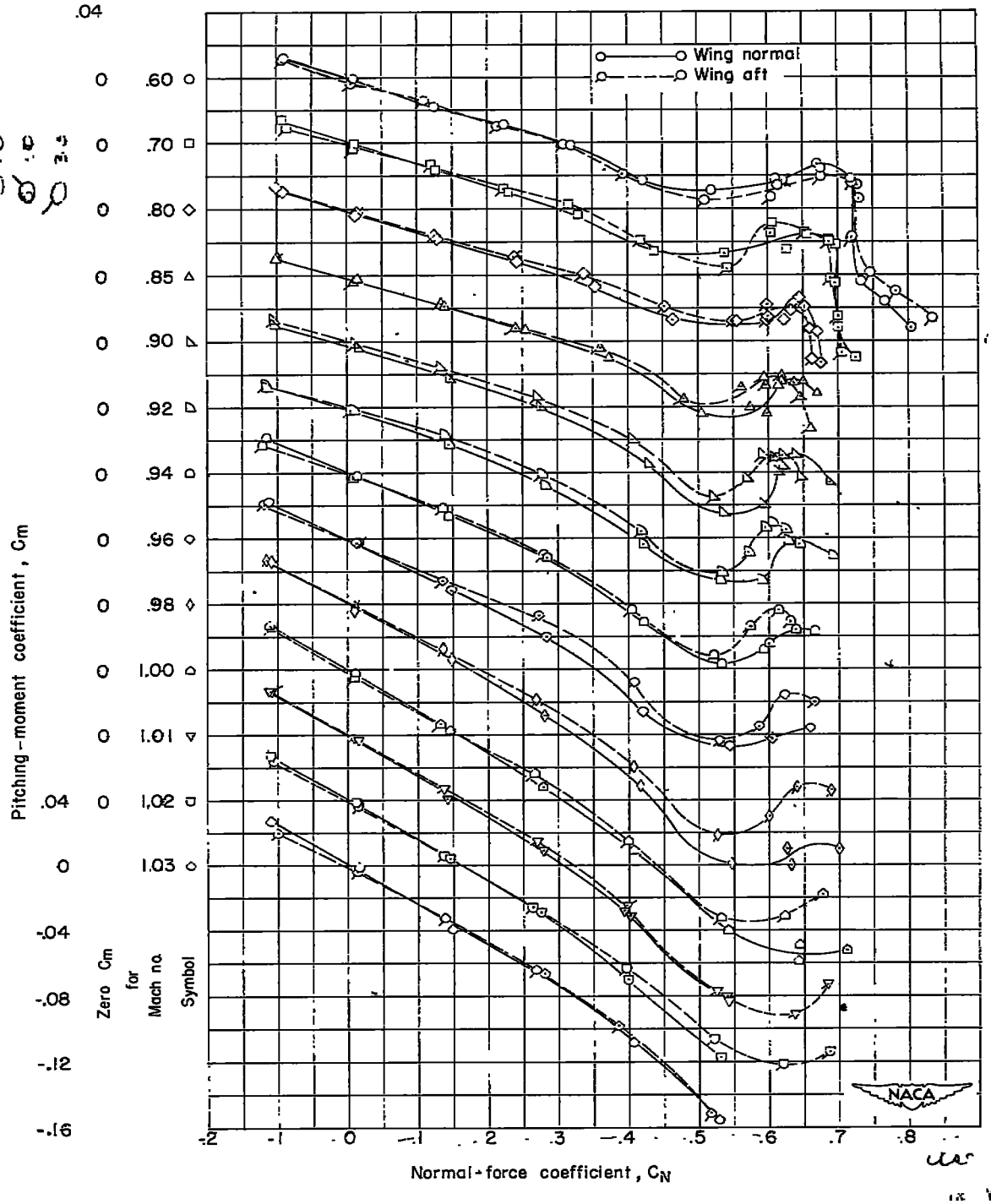

Figure 5.- The effect of wing location upon the wing pitching-moment coefficient.

[redacted]

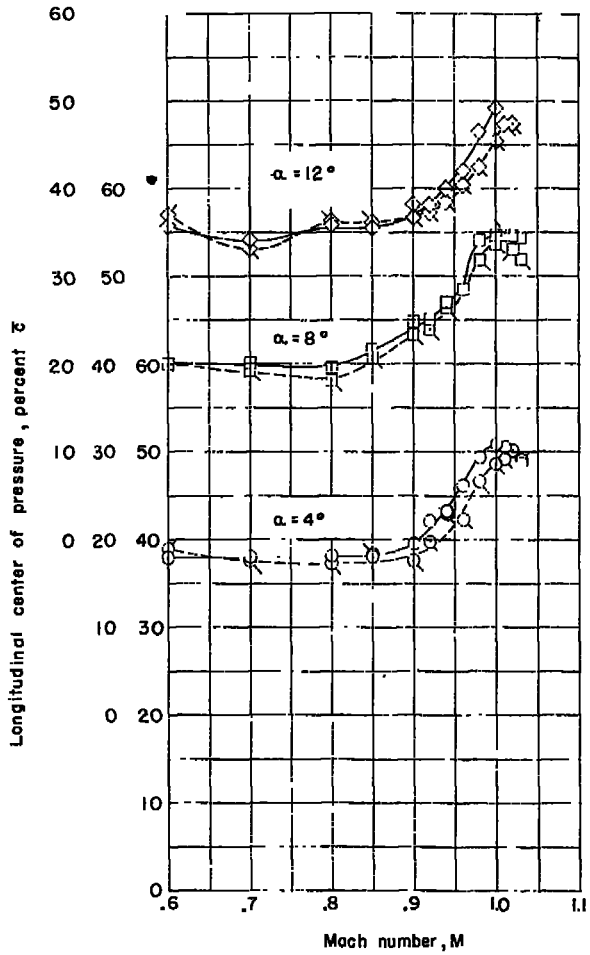

(a) Longitudinal center of pressure.

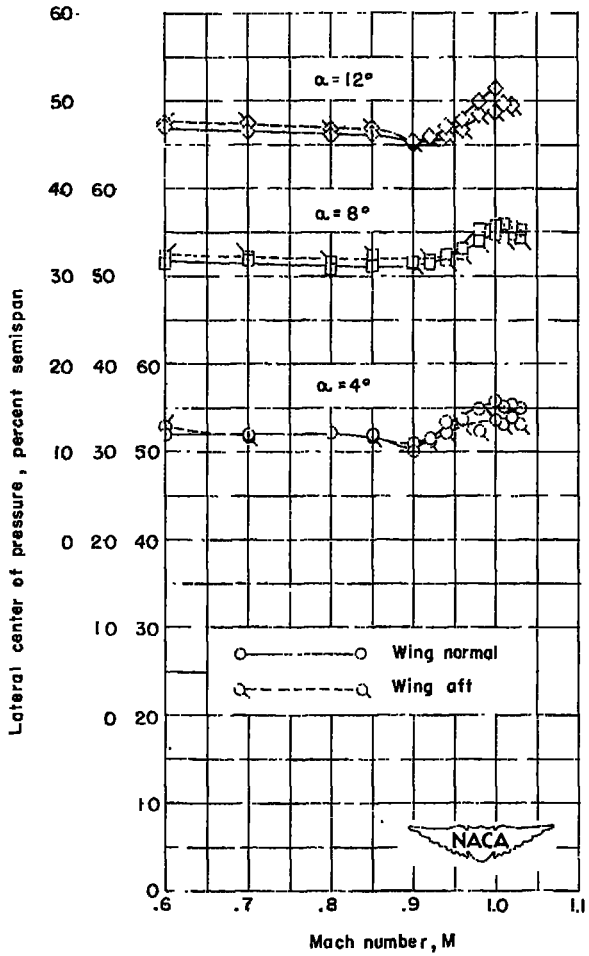

(b) Lateral center of pressure.

Figure 6.- The effect of wing location upon the location of wing longitudinal center of pressure and of wing lateral center of pressure.

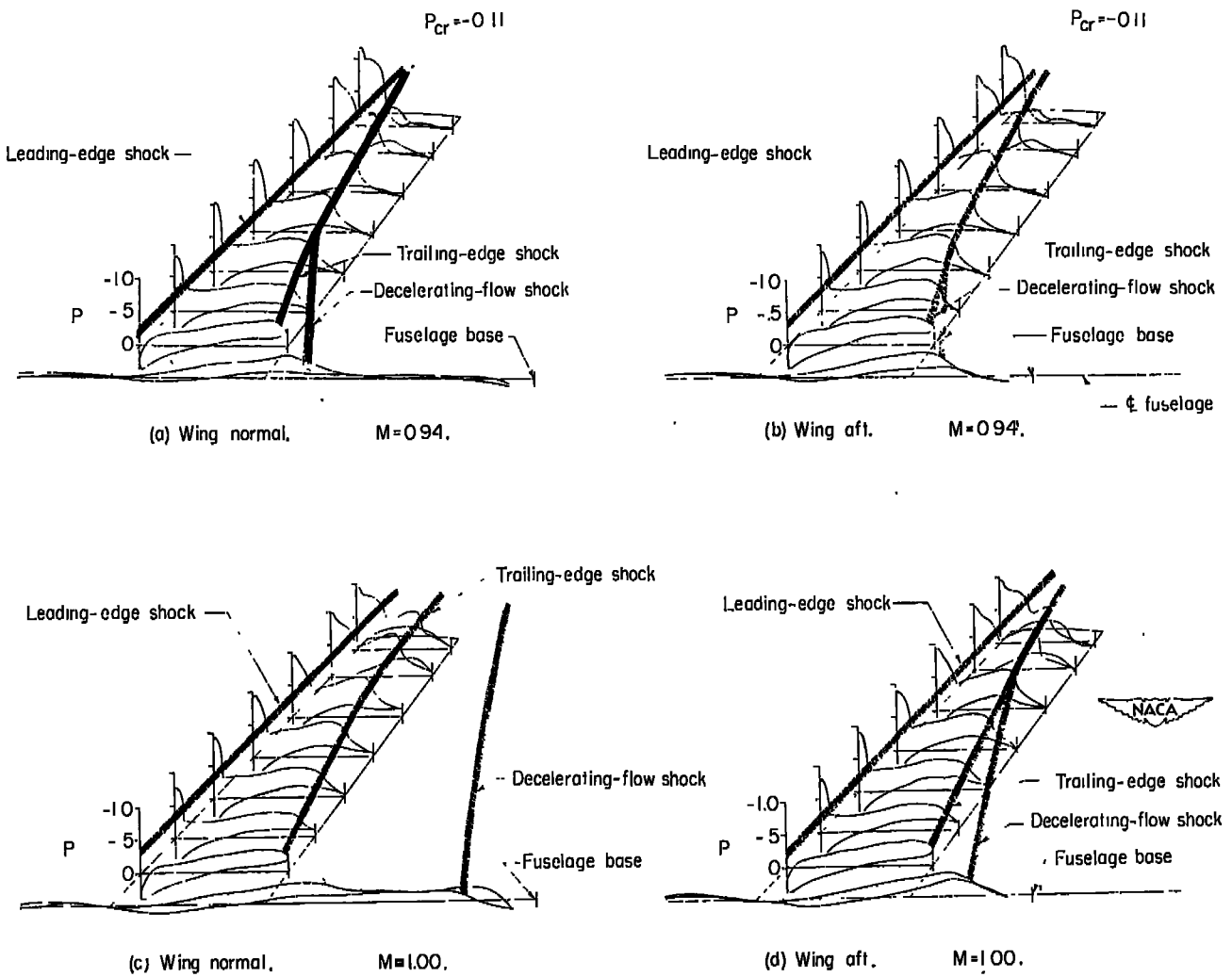

Figure 7.- Sketch showing shocks affecting the flow. To aid flow visualization, the shocks are shown on pressure contours rather than on the wing. $\alpha = 4^{\circ}$.

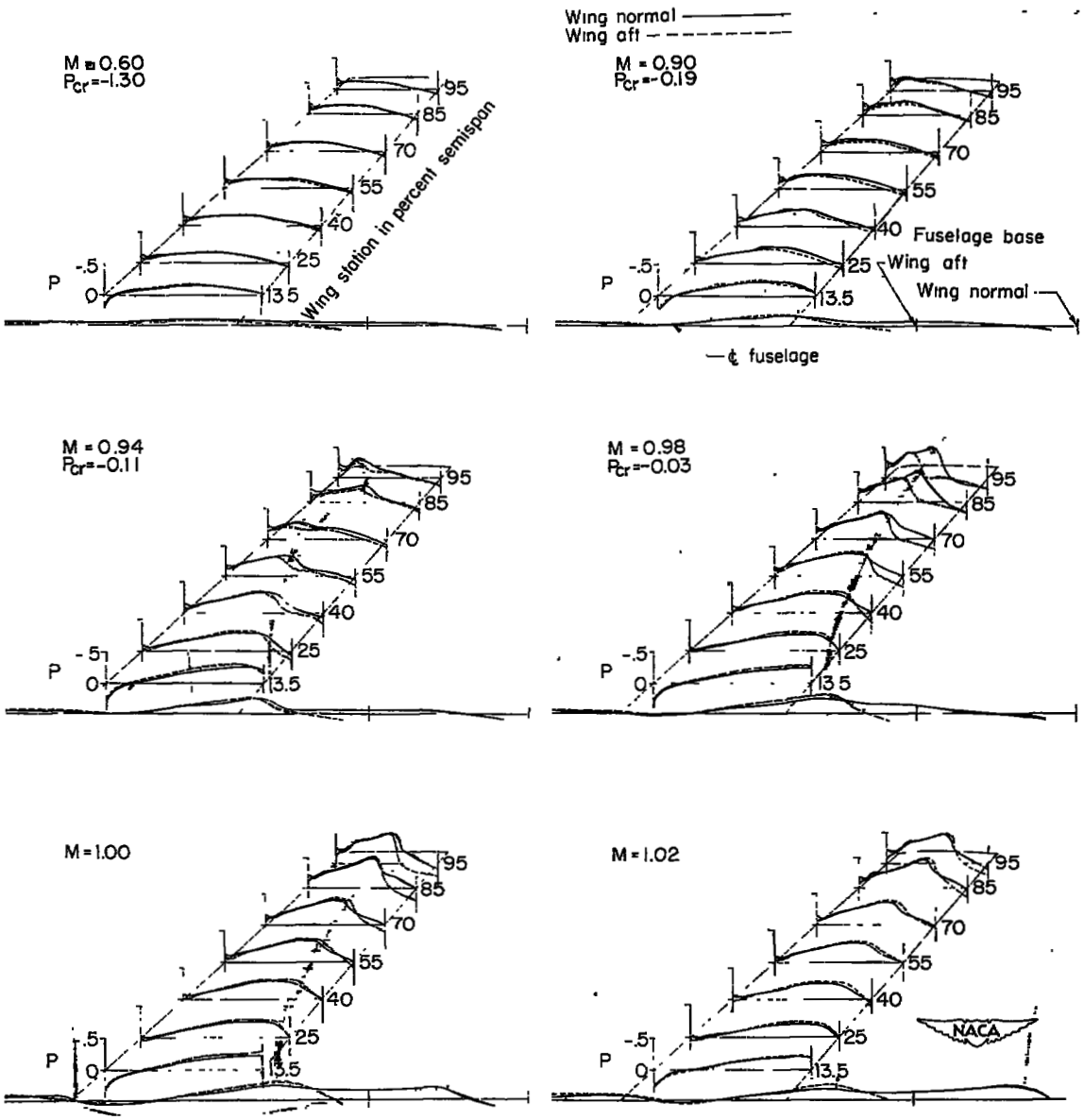

(a) Angle of attack = 0°.

Figure 8.- Chordwise pressure distributions for various Mach numbers.

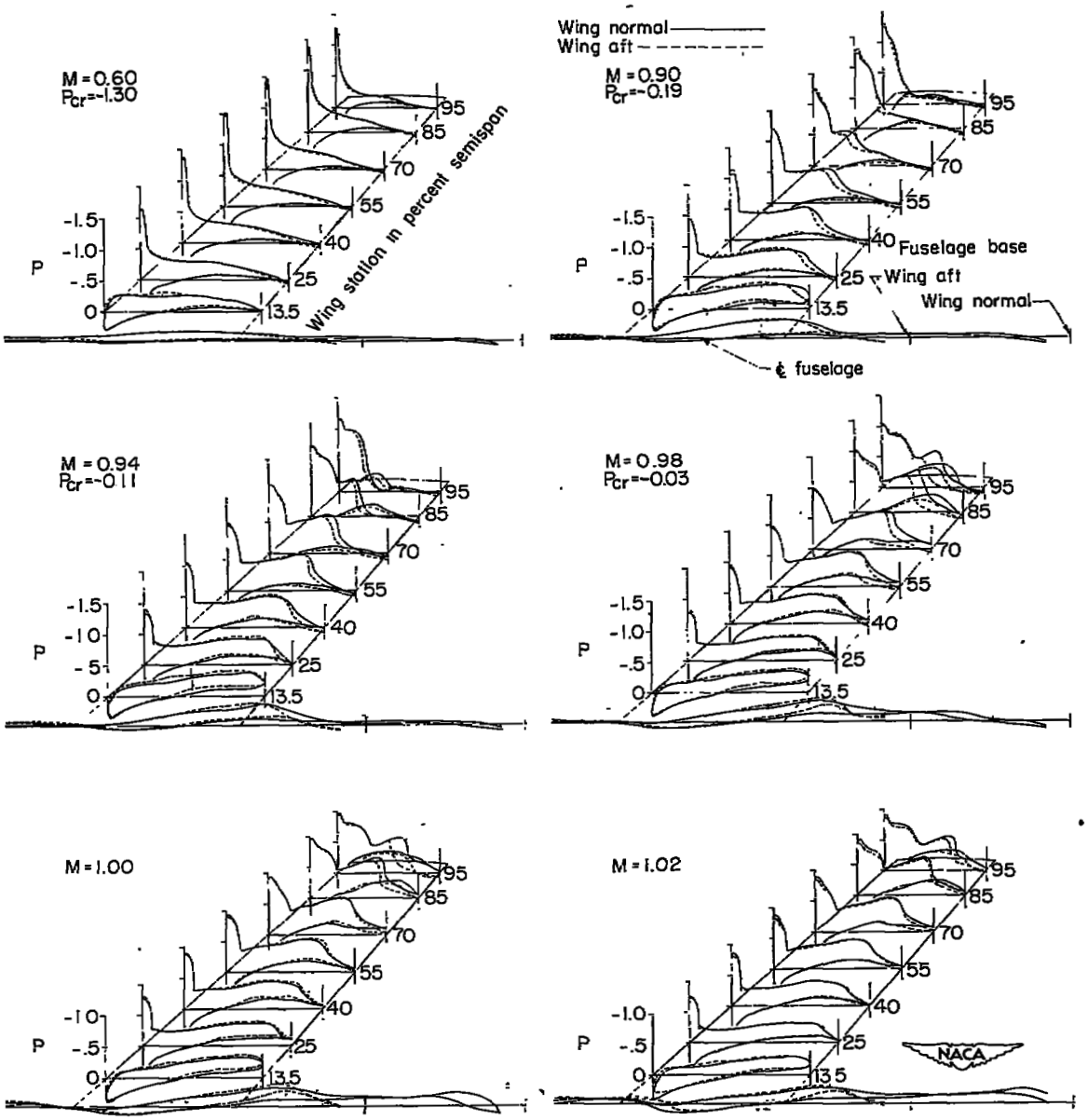

(b) Angle of attack = 4°.

Figure 8.- Continued.

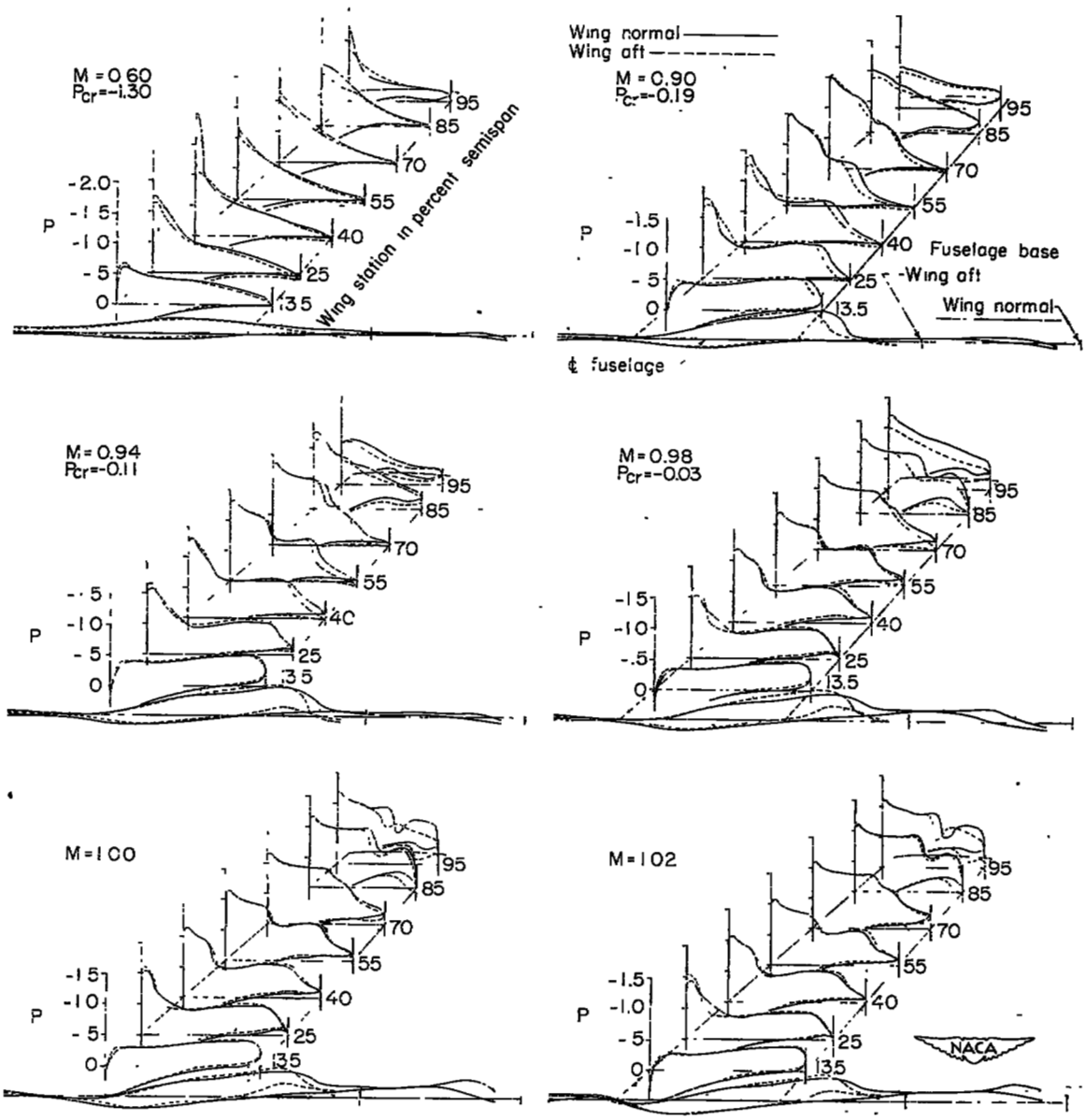

(c) Angle of attack = 8°.

Figure 8.- Continued.

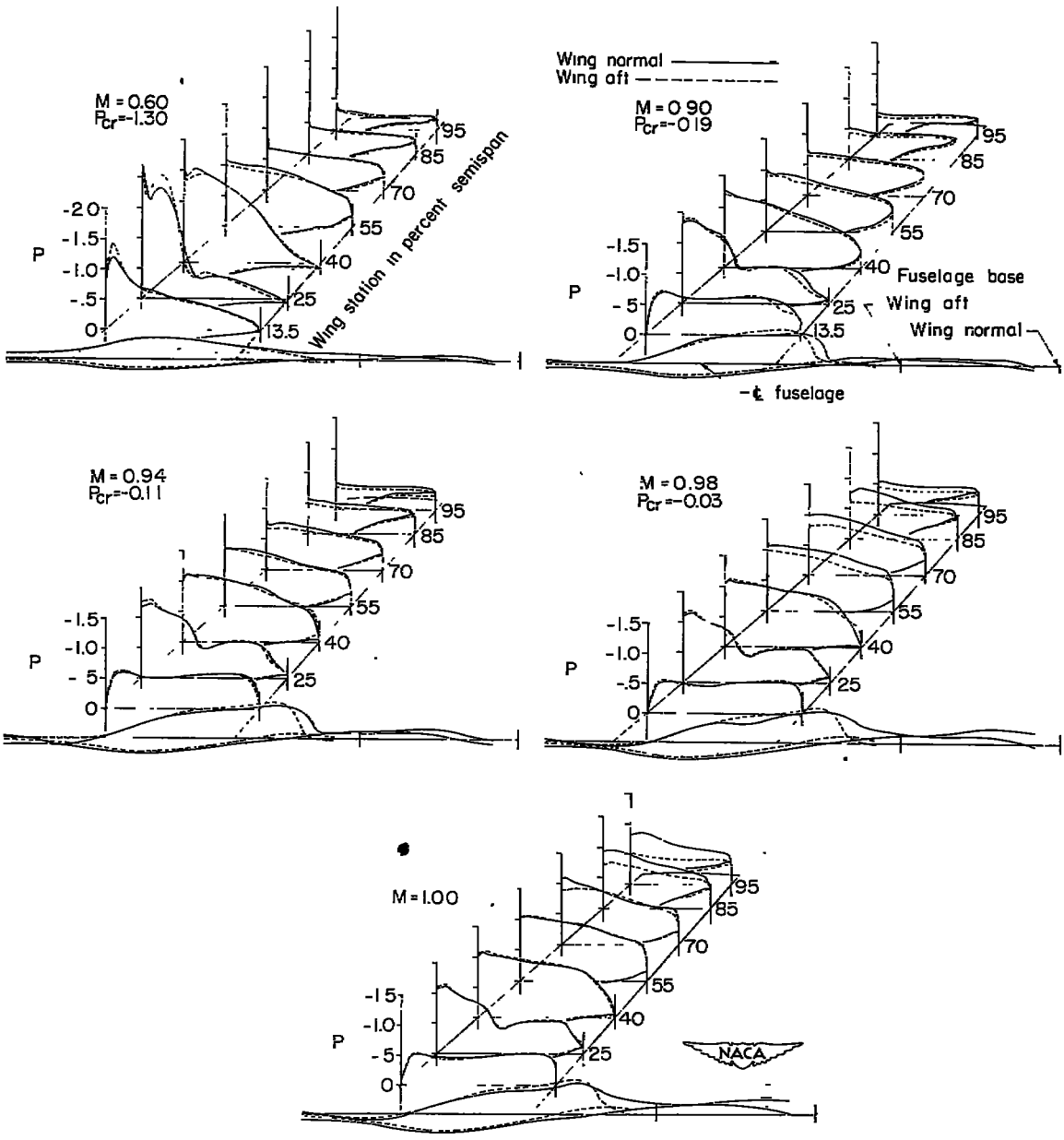

(d) Angle of attack = 12°.

Figure 8.- Concluded.

[redacted]

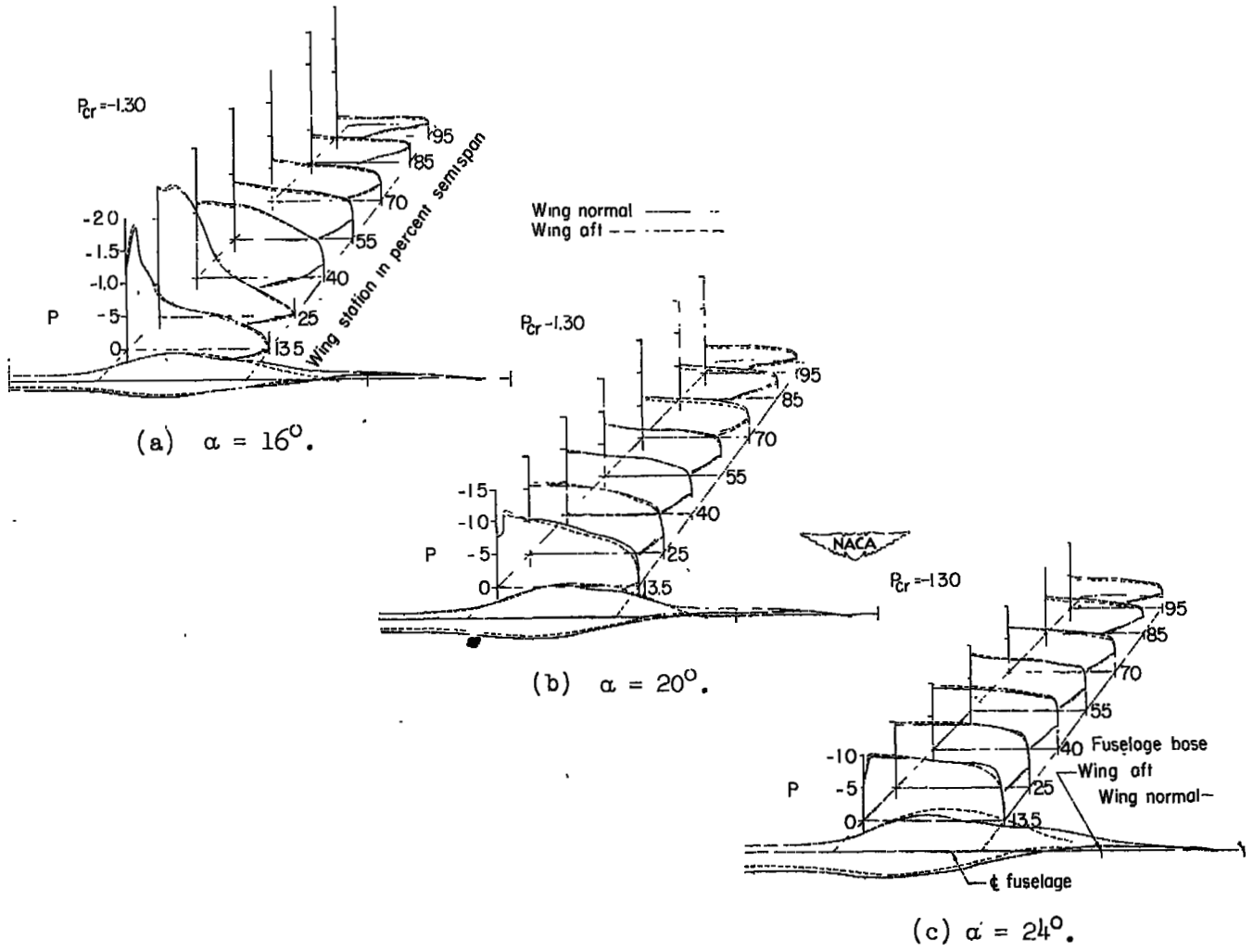

Figure 9.- Chordwise pressure distributions at higher angles of attack.
Mach number = 0.60.

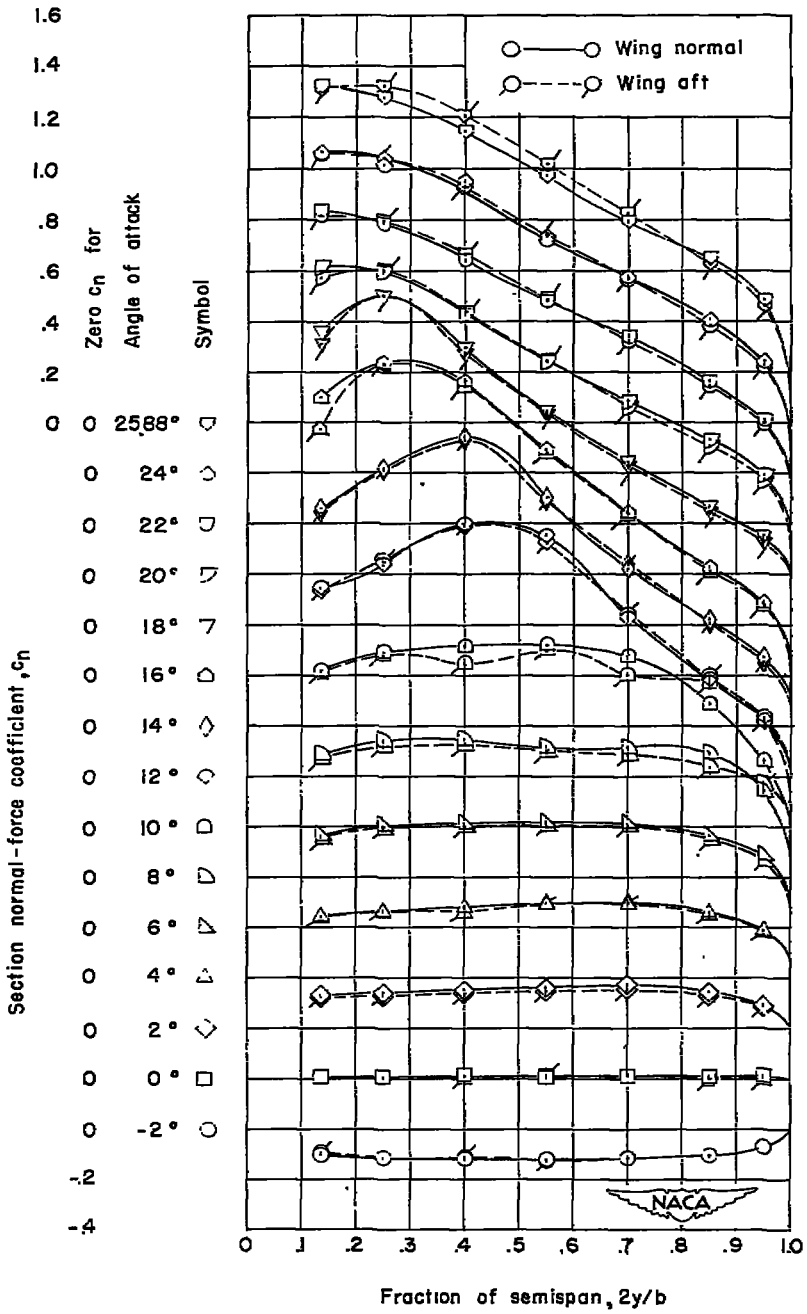

(a) M = 0.60.

Figure 10.- The effect of wing location upon section normal-force coefficient.

[redacted]

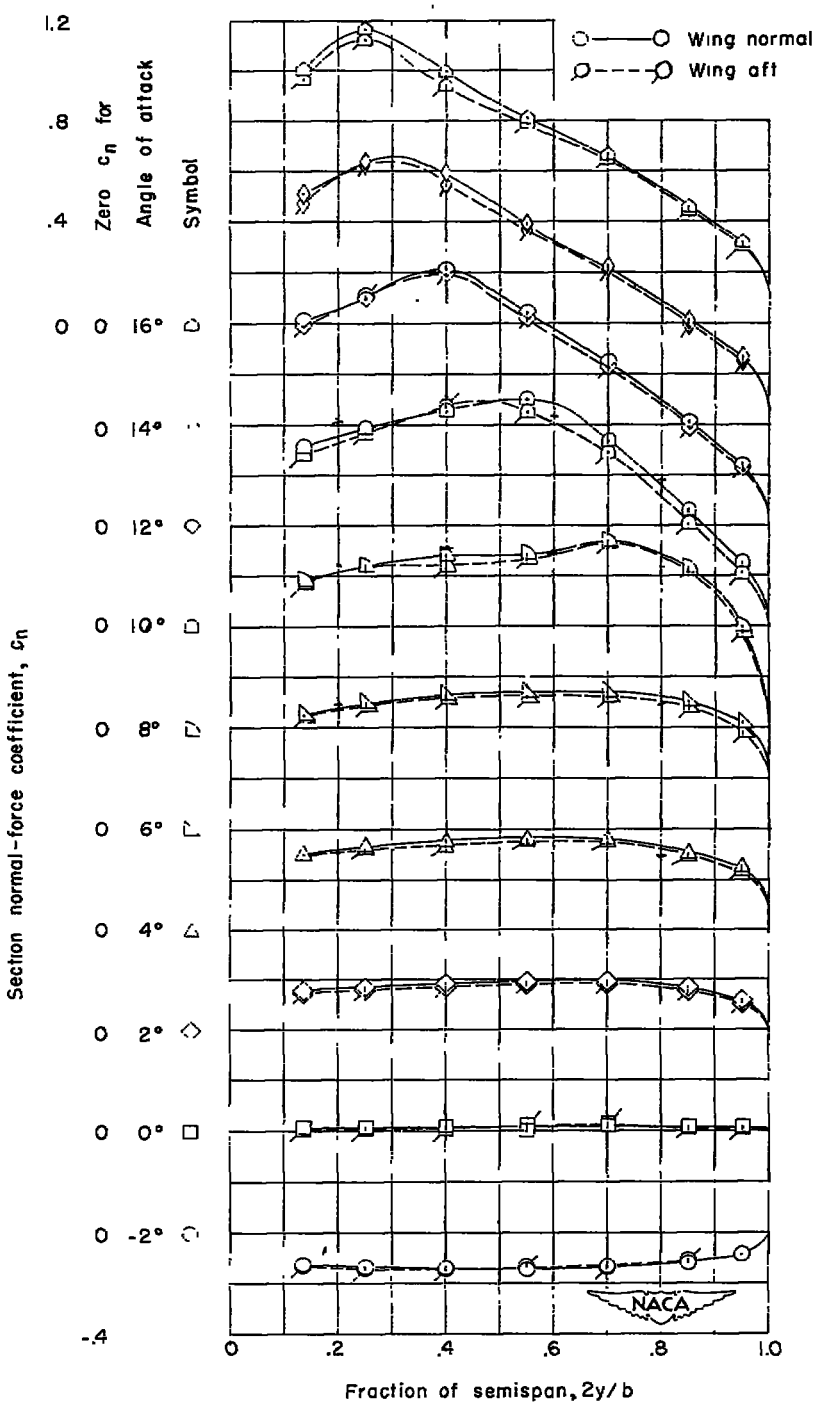

(b) M = 0.90.

Figure 10.- Continued.

[redacted]

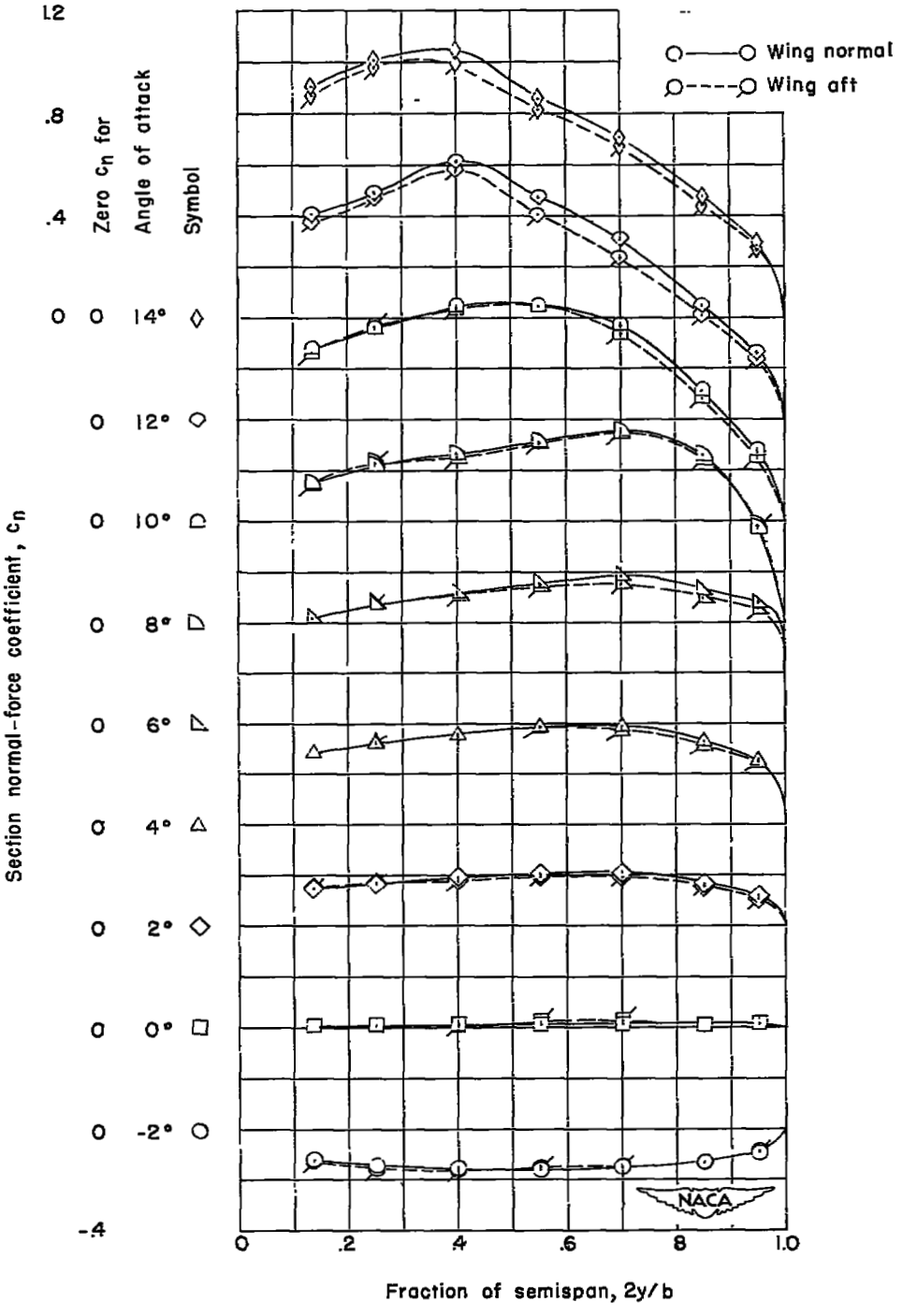

(c) M = 0.94.

Figure 10.- Continued.

[redacted]

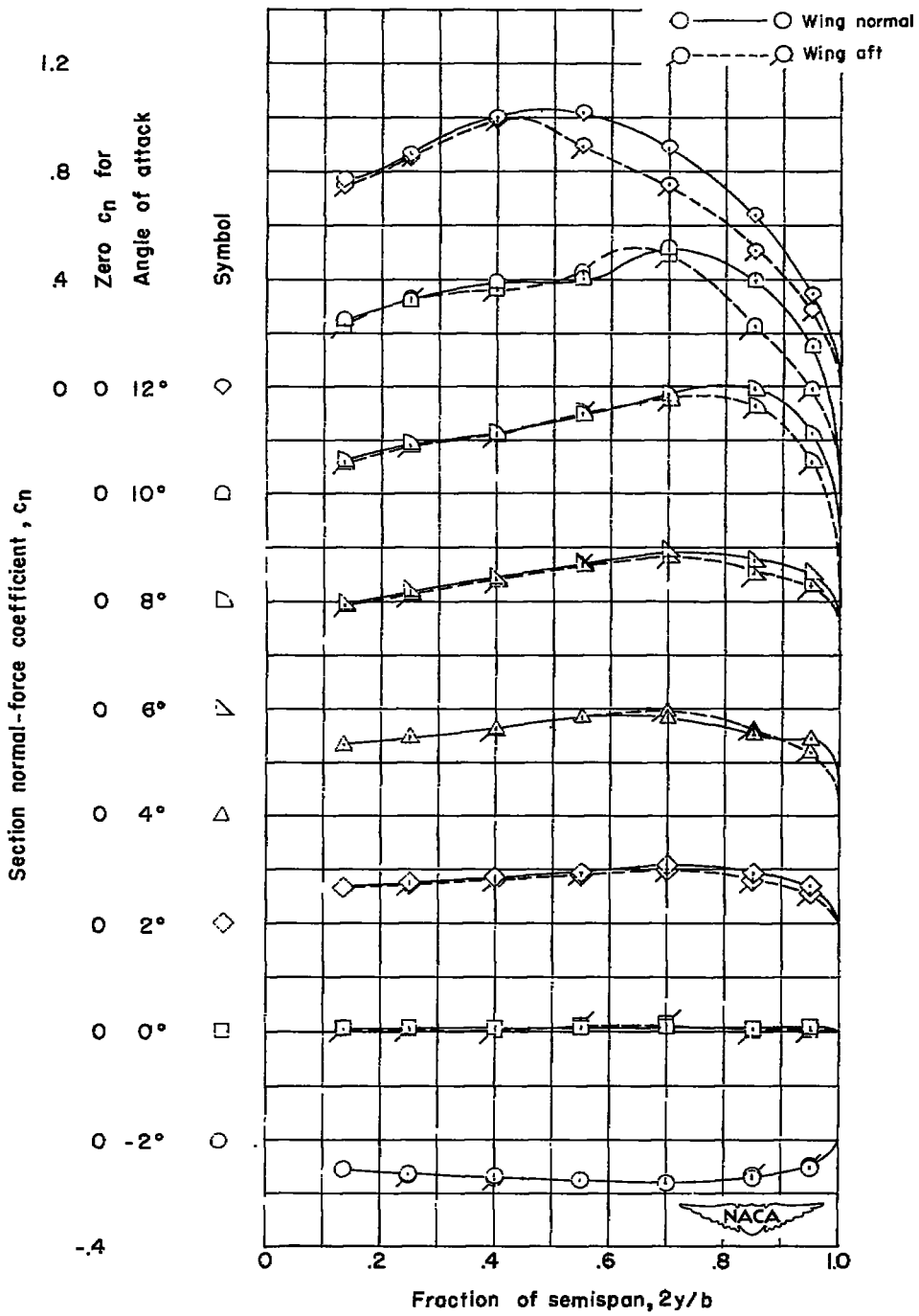

(d) M = 0.98.

Figure 10.- Continued.

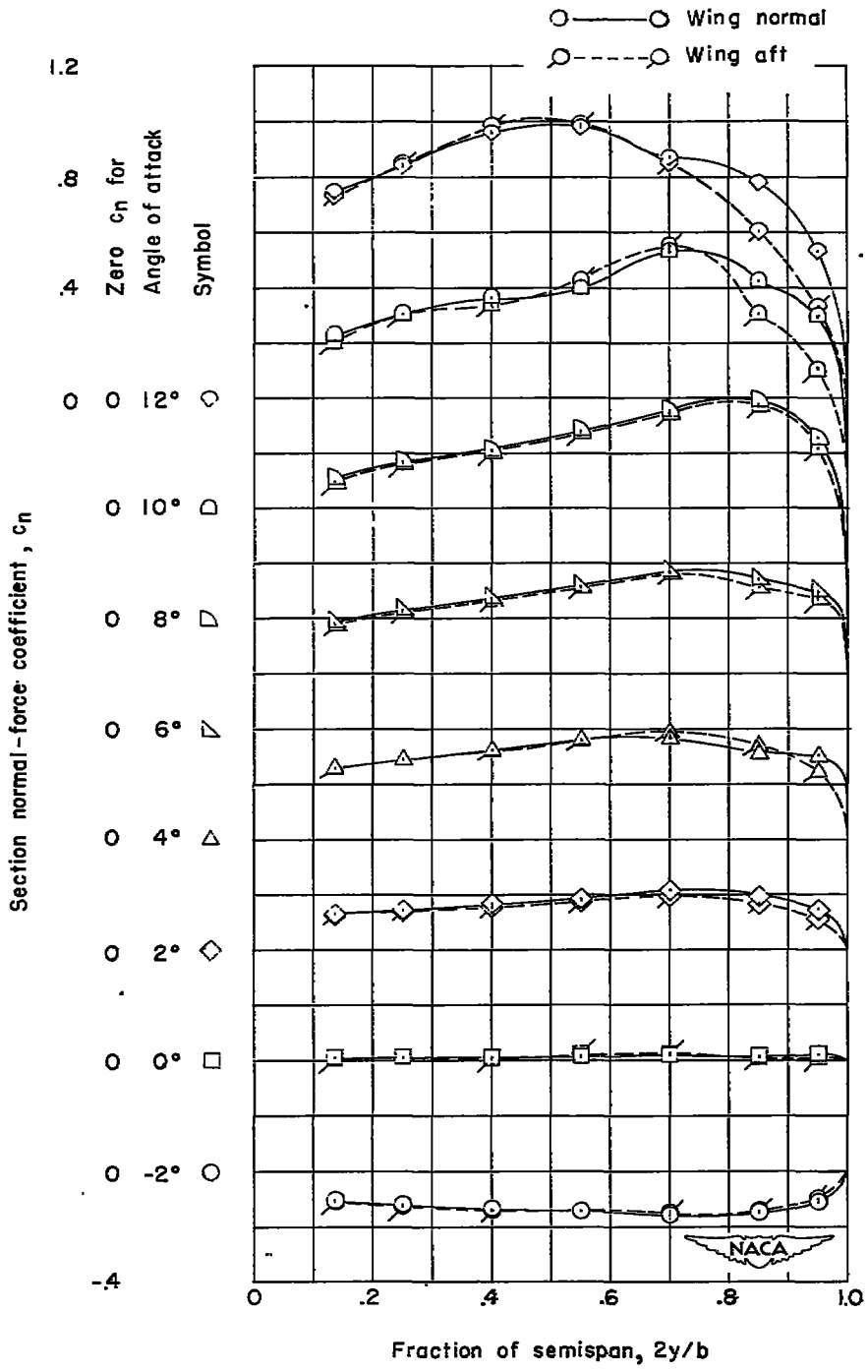

(e) M = 1.00.

Figure 10.- Continued.

[redacted]

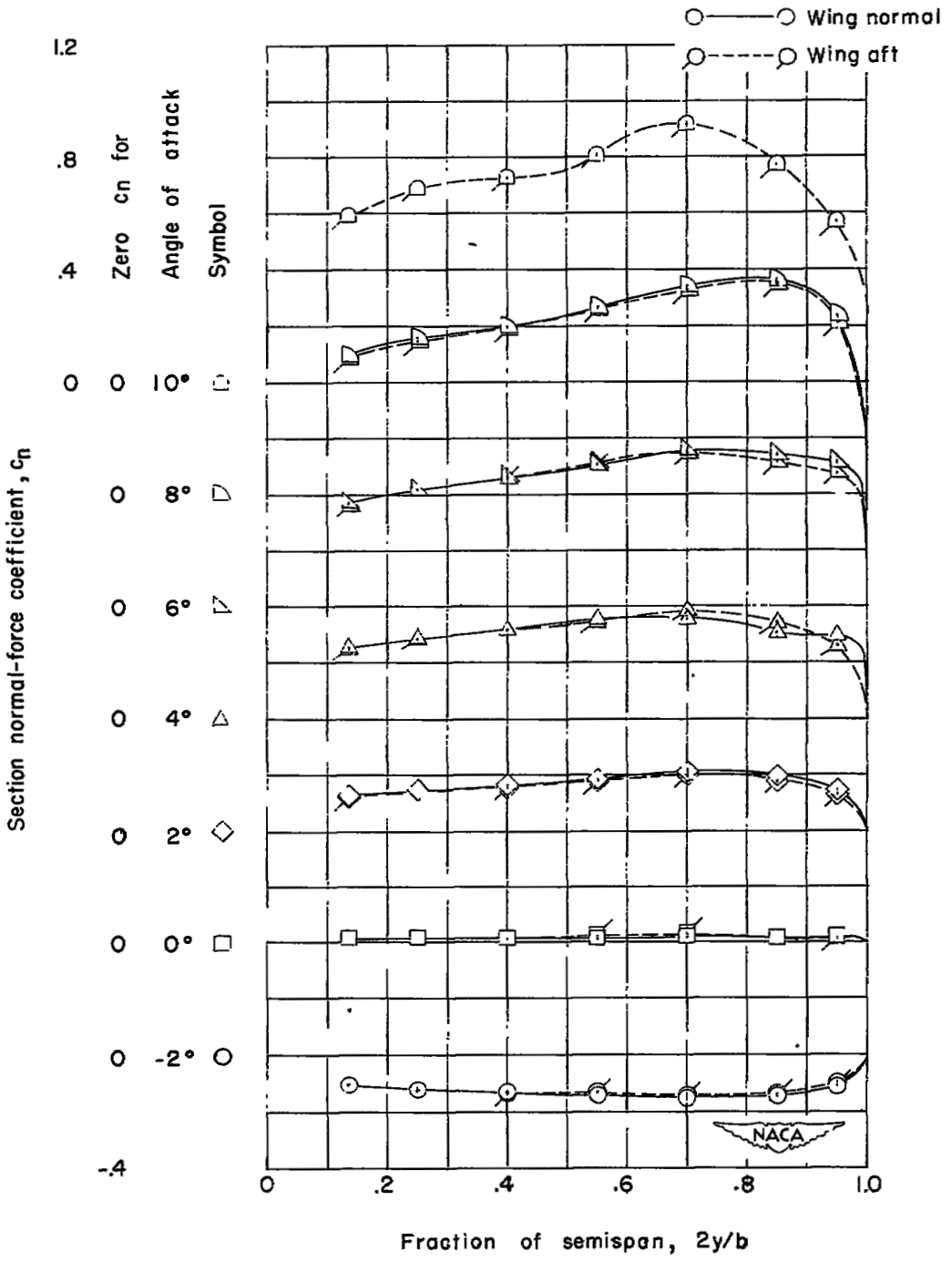

(f) M = 1.02.

Figure 10.- Concluded.

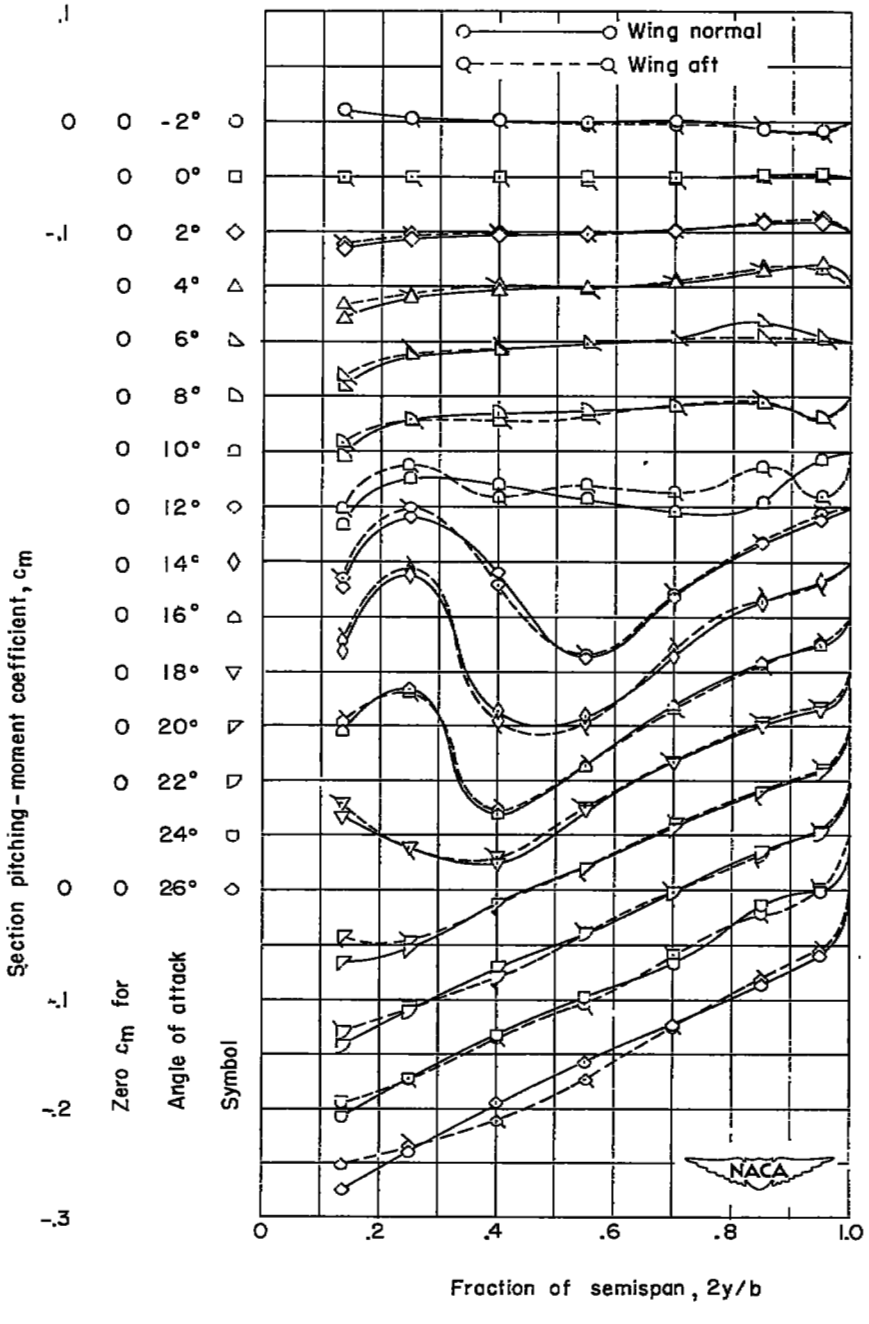

(a) M = 0.60.

Figure 11.- The effect of wing location upon the wing-section pitching-moment coefficient.

[redacted]

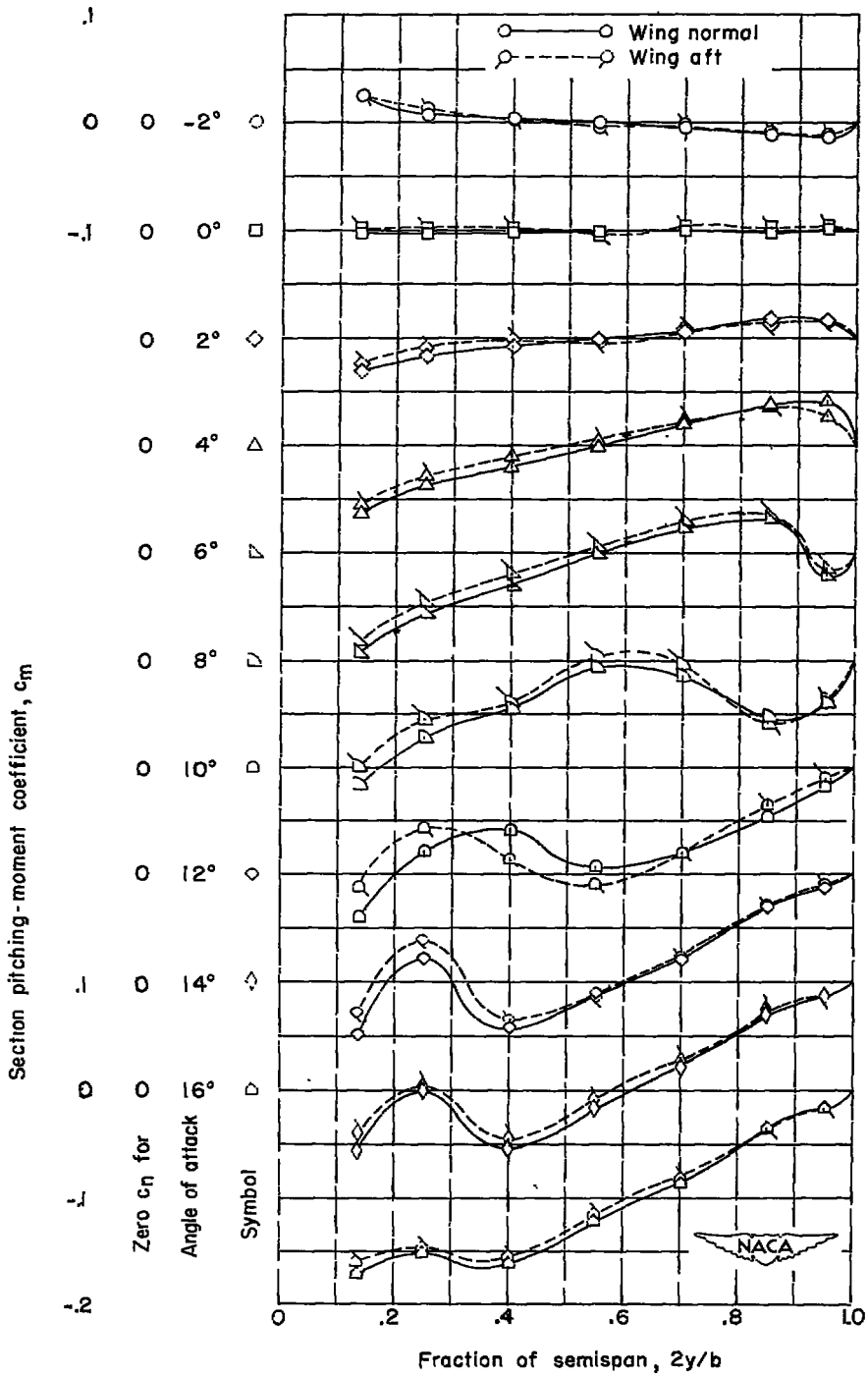

(b) M = 0.90.

Figure 11.- Continued.

[redacted]

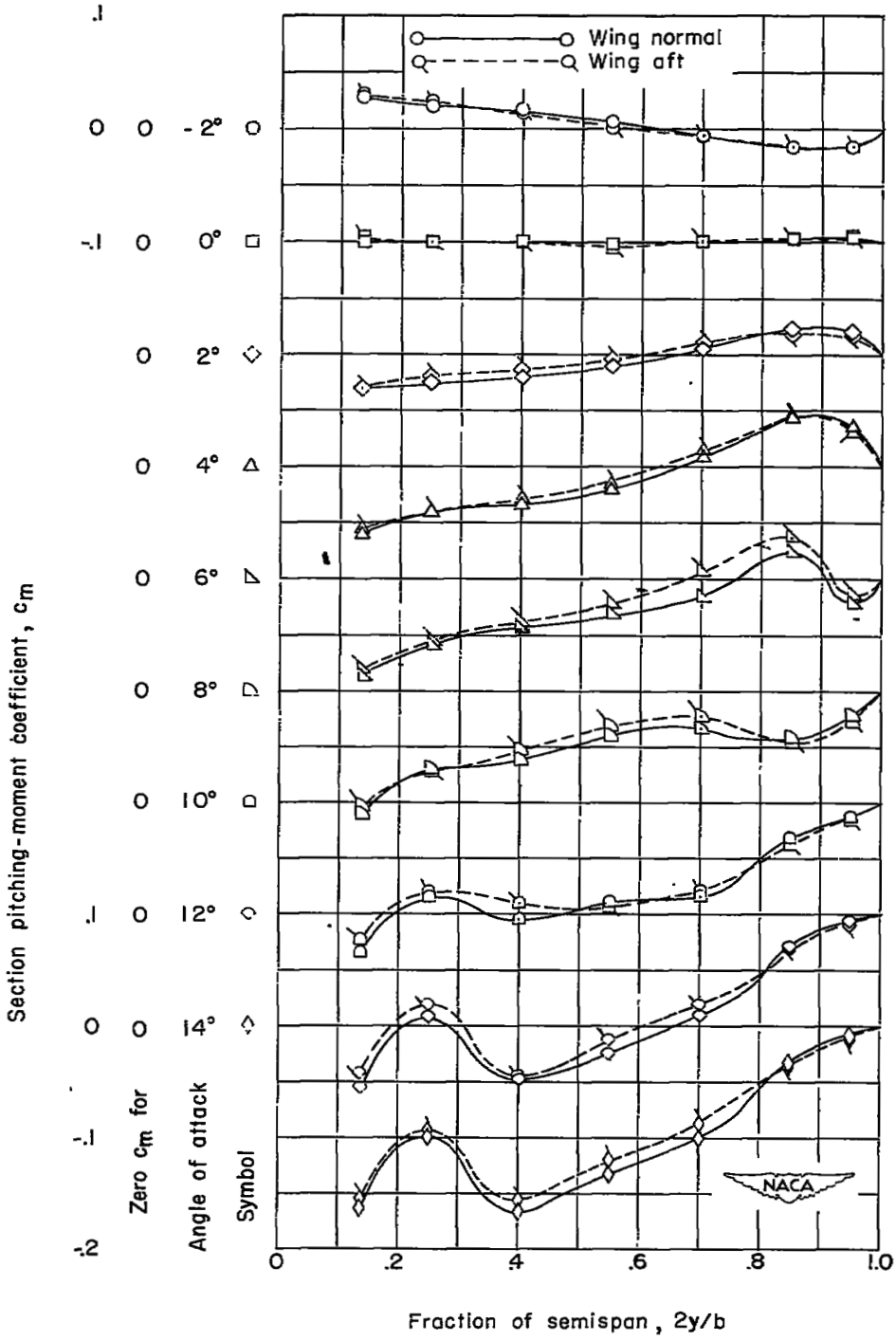

(c) M = 0.94.

Figure 11.- Continued.

[redacted]

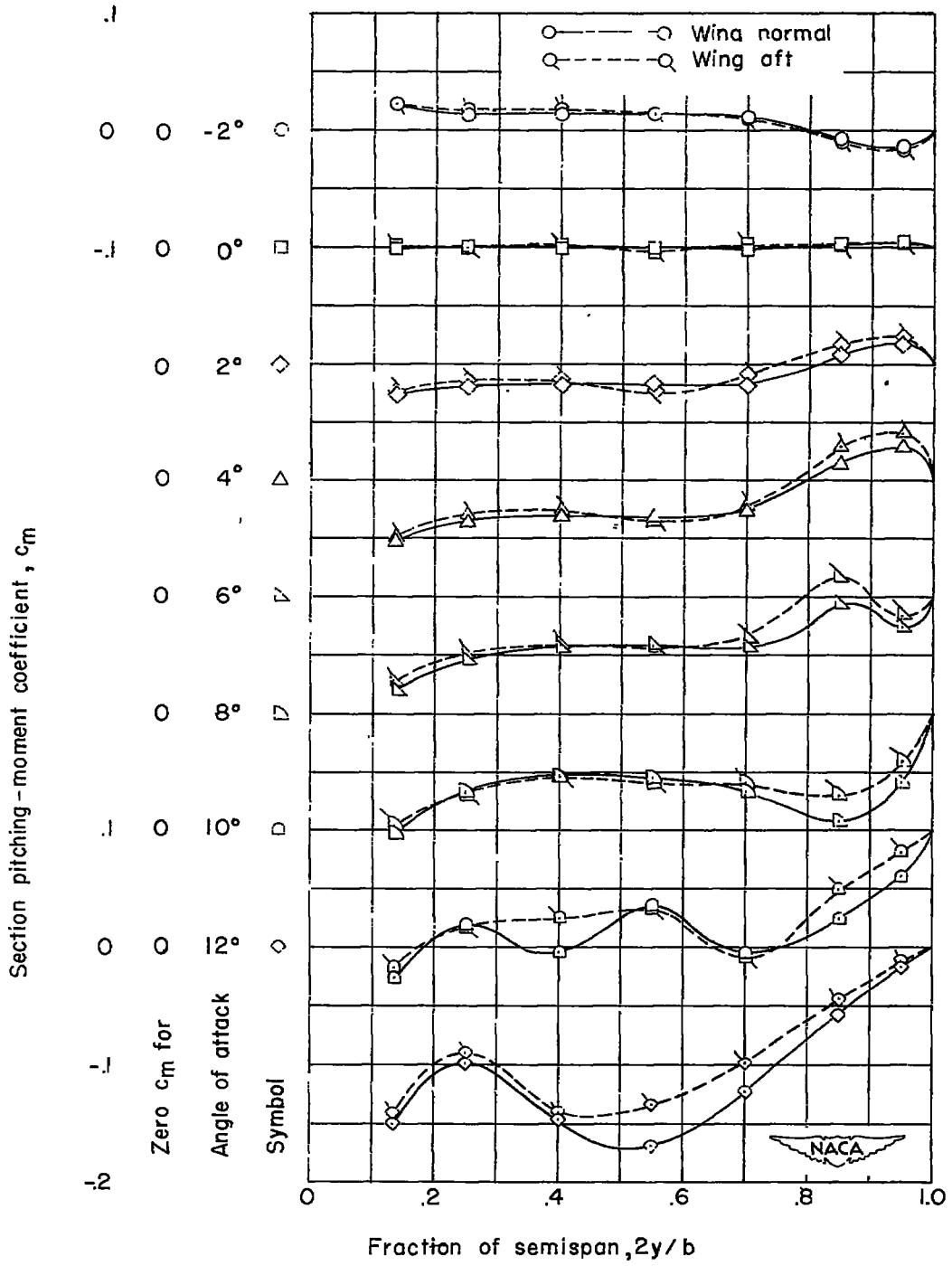

(d) M = 0.98.

Figure 11.- Continued.

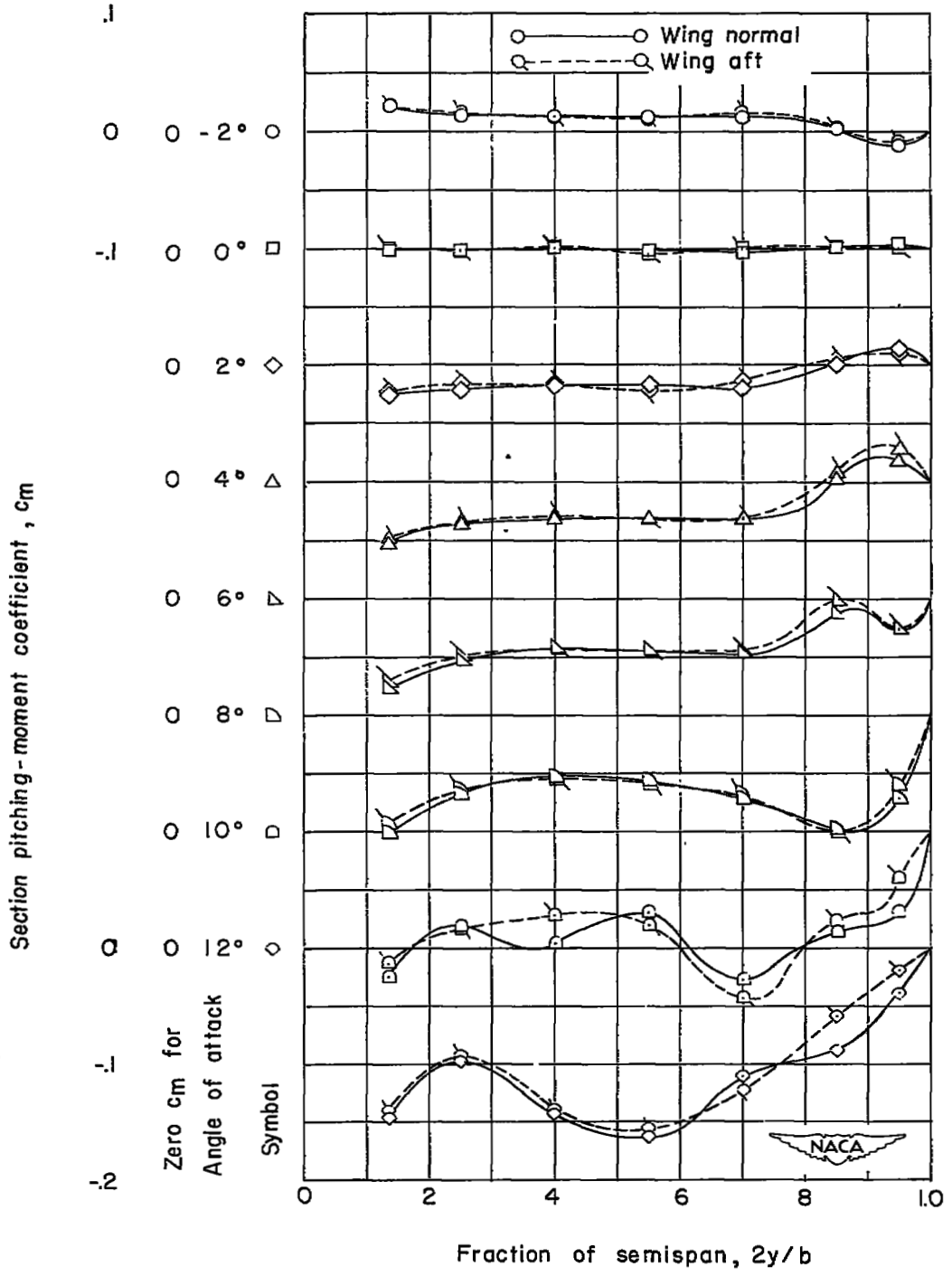

(e) M = 1.00.

Figure 11.- Continued.

[redacted]

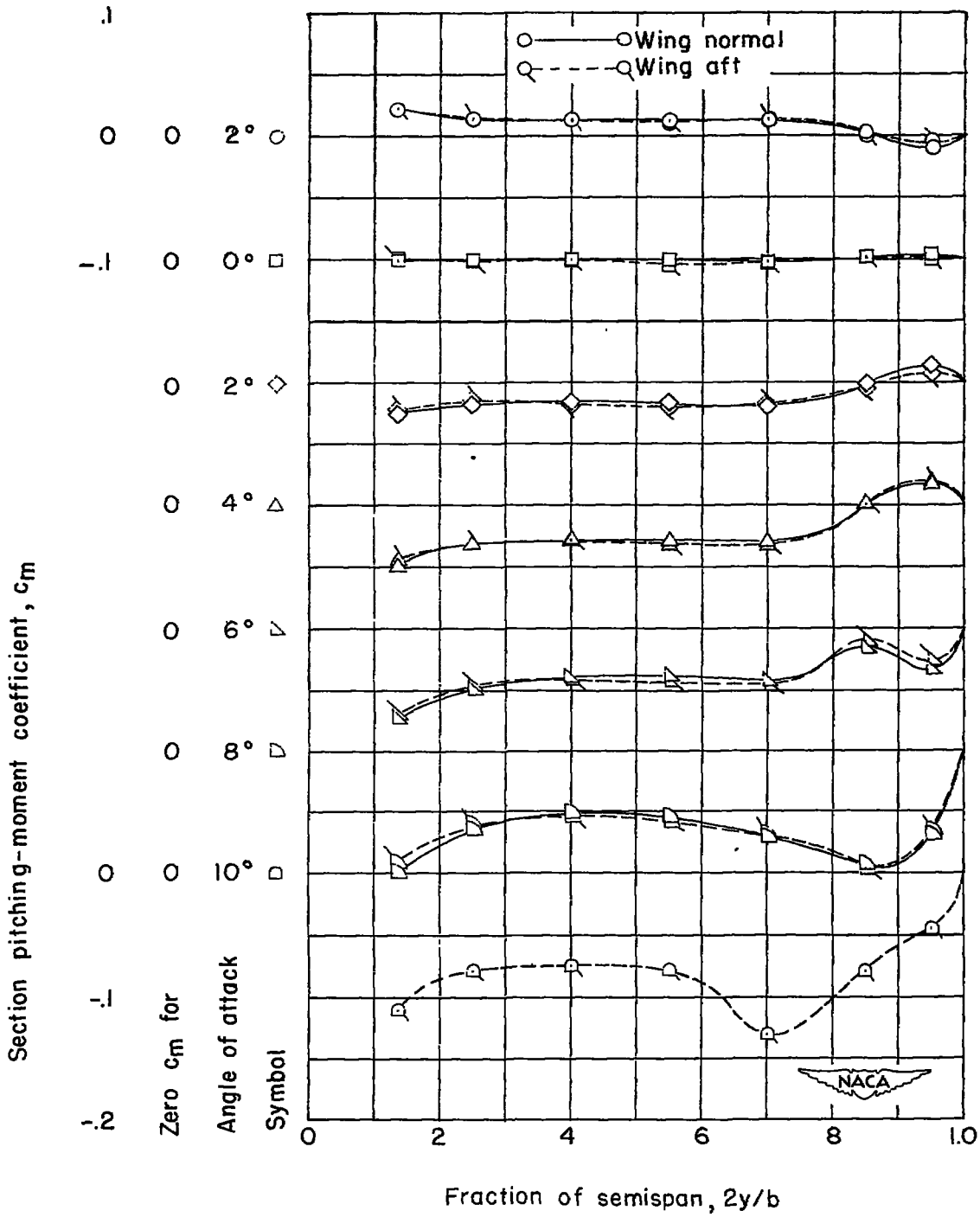

(f) M = 1.02.

Figure 11.- Concluded.

[redacted]

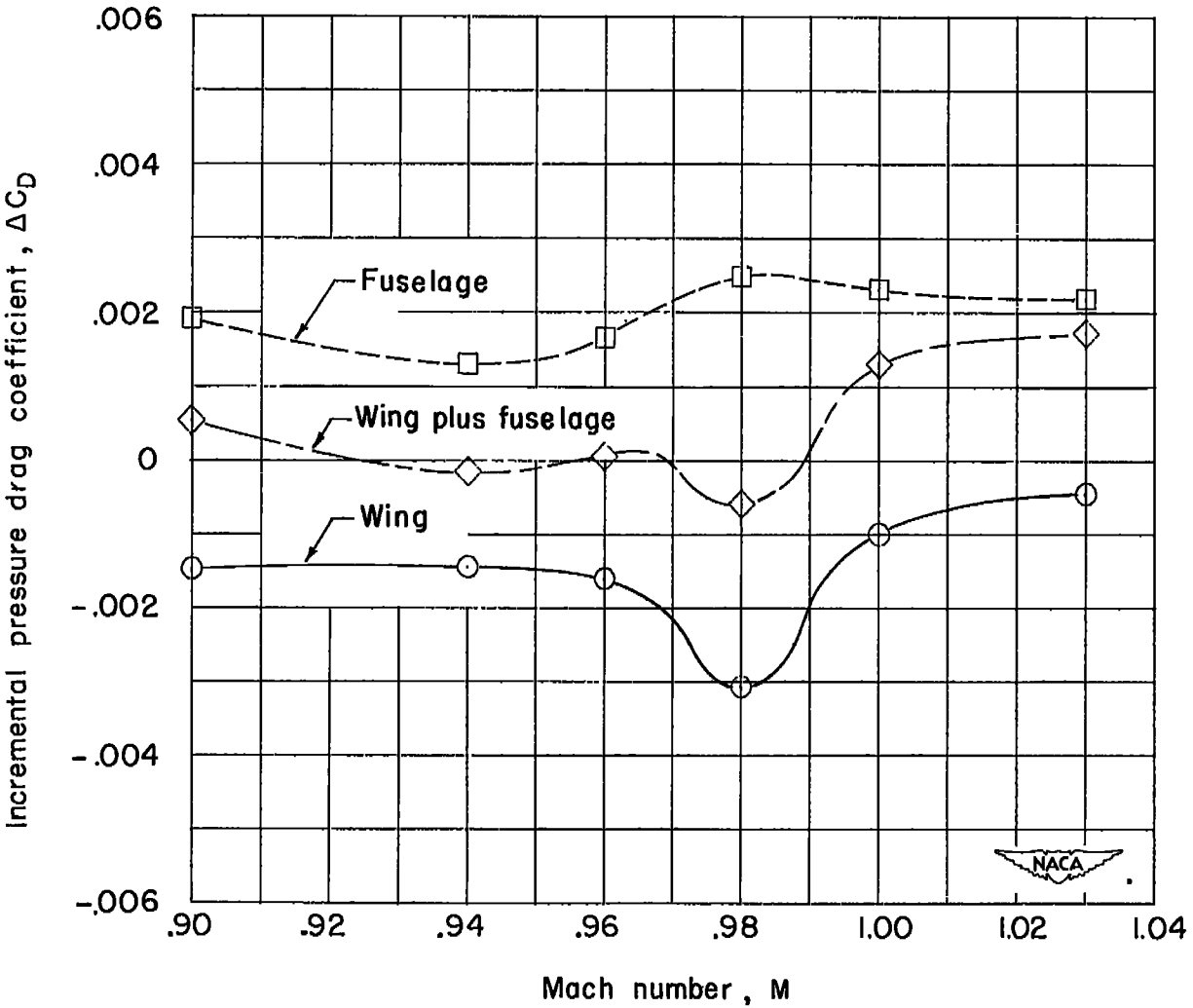

Figure 12.- Comparisons of incremental pressure drag coefficient showing the effect of wing location. $\alpha = 0^{\circ}$.

[redacted]